Committee on Earth Observation Satellites
Working Group on Calibration and Validation
Land Product Validation Subgroup

Land Surface Temperature Product Validation Best Practice Protocol

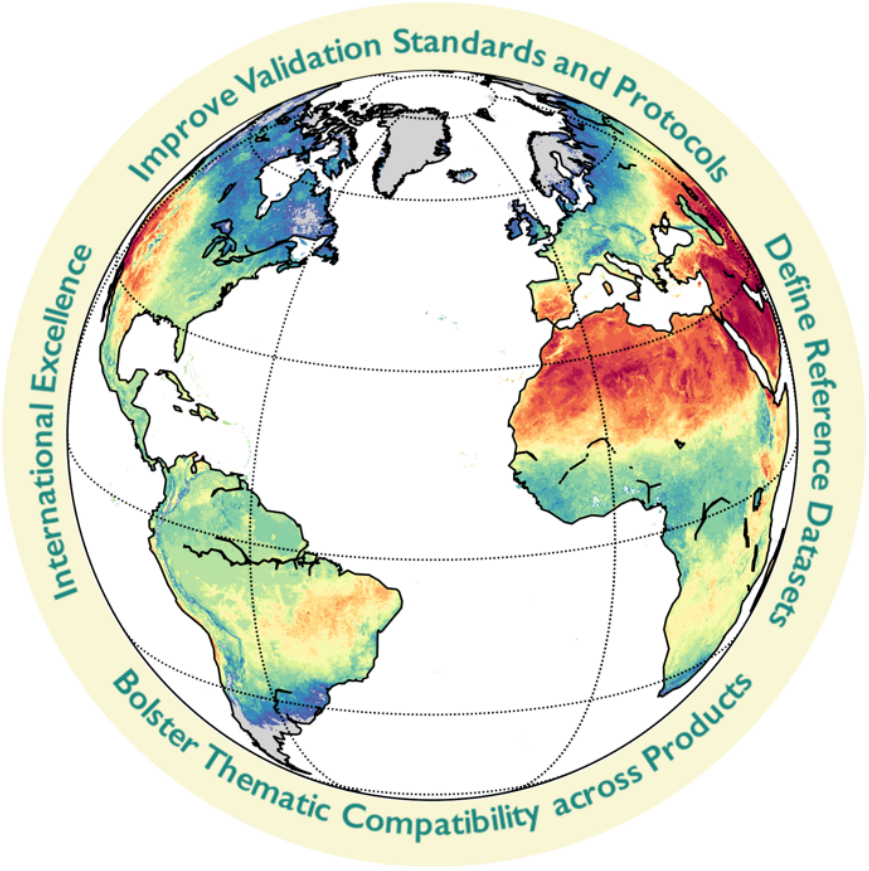

Version 1.1 - January, 2018

Editors: Pierre Guillevic, Frank Göttsche, Jaime Nickeson, Miguel Román

Authors: Pierre Guillevic, Frank Göttsche, Jaime Nickeson, Glynn Hulley, Darren Ghent, Yunyue Yu, Isabel Trigo, Simon Hook, José A. Sobrino, John Remedios, Miguel Román and Fernando Camacho

Citation: Guillevic, P., Göttsche, F., Nickeson, J., Hulley, G., Ghent, D., Yu, Y., Trigo, I., Hook, S., Sobrino, J.A., Remedios, J., Román, M. & Camacho, F. (2018). Land Surface Temperature Product Validation Best Practice Protocol. Version 1.1. In P. Guillevic, F. Göttsche, J. Nickeson & M. Román (Eds.), Good Practices for Satellite-Derived Land Product Validation (p. 58): Land Product Validation Subgroup (WGCV/CEOS), doi:10.5067/doc/ceoswgcv/lpv/lst.001

List of Revisions

Version	Revision	Date	Author
V0.0	Initial draft for internal review	April 2017	Guillevic
V1.0	CEOS LPV peer-reviewed version	October 2017	Guillevic *et al.*
V1.1	Added Appendix B	January 2018	Göttsche

Editor's Note

The editors of this document express the views of the land surface temperature (LST) and emissivity focus area of the Committee on Earth Observation Satellites (CEOS) Working Group on Calibration and Validation (WGCV) Land Product Validation (LPV) subgroup. This focus area provides those involved in the production and validation satellite-based LST products with a forum for documenting accepted best practices in an open and transparent manner. The LST product validation best practice protocol document (V1.1) presented here has undergone scientific review by remote sensing experts from across the world. All comments and suggestions have been carefully considered to formulate this consensus document, which is freely available on the LPV subgroup web site (http://lpvs.gsfc.nasa.gov/). Furthermore, a list of recommendations arising from the findings in this document is also provided at the LPV webpage. It is expected that this best practice protocol will be a living document and that recommendations within will undergo regular revisions based on community feedback and advancement in the science of LST.

We welcome all interested experts to participate in improving this document and we invite the broader community to use it for their research and applications related to LST products derived from satellite imagery. All contributors will be recognized as such in the document and on the CEOS WGCV LPV web site.

Sincerely,

The Editors:

Pierre Guillevic, University of Maryland, NASA Goddard Space Flight Center
Frank Göttsche, Karlsruhe Institute of Technology (KIT)
Jaime Nickeson, SSAI, NASA Goddard Space Flight Center
Miguel Román, NASA Goddard Space Flight Center (LPV Chair)

Chairpersons of the CEOS WGCV Land Product Validation Subgroup:

Miguel Román, NASA Goddard Space Flight Center (LPV Chair)
Fernando Camacho, EOLAB (LPV Vice-Chair)

Table of Contents

List of Figures

List of Tables

SUMMARY

The Global Climate Observing System (GCOS) has specified the need to systematically generate and validate Land Surface Temperature (LST) products. This document provides recommendations on good practices for the validation of LST products. Internationally accepted definitions of LST, emissivity and associated quantities are provided to ensure the compatibility across products and reference data sets. A survey of current validation capabilities indicates that progress is being made in terms of up-scaling and in situ measurement methods, but there is insufficient standardization with respect to performing and reporting statistically robust comparisons.

Four LST validation approaches are identified: (1) Ground-based validation, which involves comparisons with LST obtained from ground-based radiance measurements; (2) Scene-based inter-comparison of current satellite LST products with a heritage LST products; (3) Radiance-based validation, which is based on radiative transfer calculations for known atmospheric profiles and land surface emissivity; (4) Time series comparisons, which are particularly useful for detecting problems that can occur during an instrument's life, e.g. calibration drift or unrealistic outliers due to undetected clouds. Finally, the need for an open access facility for performing LST product validation as well as accessing reference LST datasets is identified.

List of Acronyms and Nomenclature

AATSR	Advanced Along-Track Scanning Radiometer
ATBD	Algorithm Theoretical Basis Document
AVHRR	Advanced Very High Resolution Radiometer
BT	Brightness Temperature
CEOS	Committee on Earth Observation Satellites
CRN	Climate Reference Network
E	Surface emissivity
ECMWF	European Center for Medium range Weather Forecasting
ECV	Essential Climate Variable (GCOS)
EPIFOV	Effective Projected Instantaneous Field of View
ESA	European Space Agency
ESU	Elementary Sampling Unit
FLUXNET	Global network of flux tower sites
FOV	Field of View
GCM	General Circulation Model
GCOS	Global Climate Observing System
GCU	Global Change Unit (at the University of Valencia)
GMAO	Global Modeling and Assimilation Office
IPCC	Inter-governmental Panel on Climate Change
ISO	International Organization for Standardization
KIT	Karlsruhe Institute of Technology
LAI	Leaf Area Index
LSA-SAF	Land Surface Analysis – Satellite Application Facility
Landsat ETM+	Landsat Enhanced Thematic Mapper +
Landsat TM	Landsat Thematic Mapper
LPV	Land Product Validation (sub-group of CEOS WGCV)
LST	Land Surface Temperature
LTER	Long Term Ecological Research Network
MAD	Median Absolute Deviation
ME	Median Error
MODAPS	MODIS Adaptive Processing System
MODIS	Moderate Resolution Imaging Spectroradiometer (NASA)
NASA	National Aeronautics and Space Administration (USA)
NCEP	National Centers for Environmental Prediction
NEON	National Environmental Observation Network (USA)
NIST	National Institute of Standards and Technology (USA)
NPL	National Physical Laboratory (UK)
OLIVE	On-Line Validation Exercise

ORNL	Oak Ridge National Laboratory (USA)
PIFOV	Ground Projected Instantaneous Field of View
PTB	Physikalisch-Technische Bundesanstalt (Germany)
QA	Quality Assessment
RMSE	Root Mean Square Error
SLSTR	Sea and Land Surface Temperature Radiometer
STD	Standard Deviation
SURFRAD	Network of surface radiation measurement sites
TIR	Thermal Infrared
TOA	Top of Atmosphere
UNFCCC	United Nations Framework Convention on Climate Change
WGCV	Working Group on Calibration and Validation (CEOS)
WMO	World Meteorological Organization

1 INTRODUCTION

This section describes the international framework that has motivated this document, describes the associated Land Surface Temperature (LST) requirements and summarizes the goals of the presented validation protocol.

1.1 Importance of Land Surface Temperature

Energy and water exchanges at the land surface – atmosphere interface have a major influence on the Earth's weather and environment. LST is a fundamental variable in the physics of land surface processes from local to global scales and is closely linked to radiative, latent and sensible heat fluxes at the surface-atmosphere interface. Thus, understanding and monitoring the dynamics of LST and its links to human induced changes is critical for modeling and predicting environmental changes due to climate variability as well as for many other applications such as geology, hydrology and vegetation monitoring. From a climate perspective, LST is important for evaluating land surface and land-atmosphere exchange processes, constraining surface energy budgets and model parameters, and providing observations of surface temperature change both globally and in key regions. LST has been used for monitoring climate warming trends over Greenland (Hall *et al.*, 2012), inland water bodies (Schneider and Hook, 2010), and more recently in urban areas (Malakar and Hulley, 2016). Numerical models ranging from local to global scales represent and predict effects of surface fluxes. LST versatility has been previously demonstrated in a wide variety of Earth science research over the past two decades, including reducing and understanding systematic biases in land surface models (Zhou *et al.*, 2003; Zheng *et al.*, 2012; Trigo *et al.*, 2015; Orth *et al.*, 2017), filling gaps where few in situ measurements of surface air temperatures exist (e.g. over Africa). Human health studies include estimating urban heat island effects (Dousset and Gourmelon, 2003; Sobrino *et al.*, 2013; Luvall *et al.*, 2015), spatial mapping of heat waves in urban and rural regions (Dousset *et al.*, 2011; Krehbiel and Henebry, 2016), and epidemiological studies about the exposure risk to Lyme and tick-borne encephalitis (Randolph *et al.*, 2000; Neteler, 2005). LST has also been used for predicting the most favorable areas for vector-borne diseases, e.g. from Asian tiger mosquito outbreaks in Europe (Neteler *et al.*, 2011). In the agricultural sector, LST has been used to detect and characterize droughts, plant stress and water consumptive use (Kogan 1995, 1997; Singh *et al.*, 2003; Fisher *et al.*, 2008; Rojas *et al.*, 2011; Anderson *et al.*, 2011a; Hain *et al.*, 2011; Gallego-Elvira *et al.*, 2013; Mu *et al.*, 2013; Anderson *et al.*, 2016a, 2016b and Semmens *et al.*, 2016), surface hydrology and evapotranspiration retrieval (Sandholt *et al.*, 2002; Nishida *et al.*, 2003; Cleugh *et al.*, 2007; Kalma *et al.*, 2008; Anderson *et al.*, 1997, 2011b, 2012; Allen *et al.*, 2007). From LST daily time series, indices for mapping heat requirements for grapevine varieties can be calculated to characterize potential growing regions for viticulture (Zorer *et al.*, 2013), in addition to being able to predict crop ripening (Hall and Jones, 2010; Jones *et al.*, 2010) and insect infestations (Pasotti *et al.*, 2006; da Silva et al, 2015). Other direct practical applications of LST concern land-cover change analyses (Lambin and Ehrlich, 1997; Barbosa *et al.*, 1998), the derivation of snow cover and wetness maps (Basist *et al.*, 1998), the detection of fundamental changes in land-surface energy partioning (Mildrexler *et al.*, 2007), land cover classification (Roy 1997), thermal inertia (Sobrino and El Kharraz, 1999) and cloud detection (Jedlovec *et*

al., 2008; Stöckli, 2013). More than 30 thermal infrared applications were identified in Sobrino *et al.* (2016). Furthermore, spectral emissivity, an important variable that is used to derive LST and is often retrieved together with the LST, can be used to monitor and assess melt zones on glaciers, and in detecting land cover change and degradation (Hulley *et al.*, 2014).

1.2 The UNFCCC and the Global Climate Observing System

Worldwide systematic observation of the climate system is required for advancing scientific knowledge on changes to our climate. The United Nations Framework Convention on Climate Change (UNFCCC) calls on the Parties to promote and cooperate in this systematic observation of the climate system, including support of existing international programs and networks, as indicated in Articles 4.1(g) and 5 of the Convention. A key dimension for the implementation of those Articles has been the cooperation with the Global Climate Observing System (GCOS), a joint undertaking of the World Meteorological Organization (WMO), the Intergovernmental Oceanographic Commission (IOC) of the United Nations Educational Scientific and Cultural Organization (UNESCO), the United Nations Environment Programme (UNEP) and the International Council for Science (ICSU) with its secretariat hosted by the WMO, reinforced by decisions taken at various Conferences of the Parties. The signatories of the UNFCCC have thus adopted the GCOS as the organizing body for climate observations expressed through its Implementation Plans (GCOS-82, GCOS-200). These Implementation Plans establish the requirements for the systematic monitoring of a suite of Essential Climate Variables (ECV) globally. Land Surface Temperature (LST) is one of the terrestrial ECVs recognized by GCOS (GCOS-200).

1.3 The Role of CEOS WGCV

LST can be measured in situ and from remote observations. While it is routinely measured at a number of research sites, the measurement network is sparse in many regions of the world. Figure 1 presents different networks or individual sites currently used to validate LST standard products derived from US and European instruments (as of September 2017). This dataset should be maintained and ideally expanded to become much more representative of the diversity of ecosystem and climatic conditions.

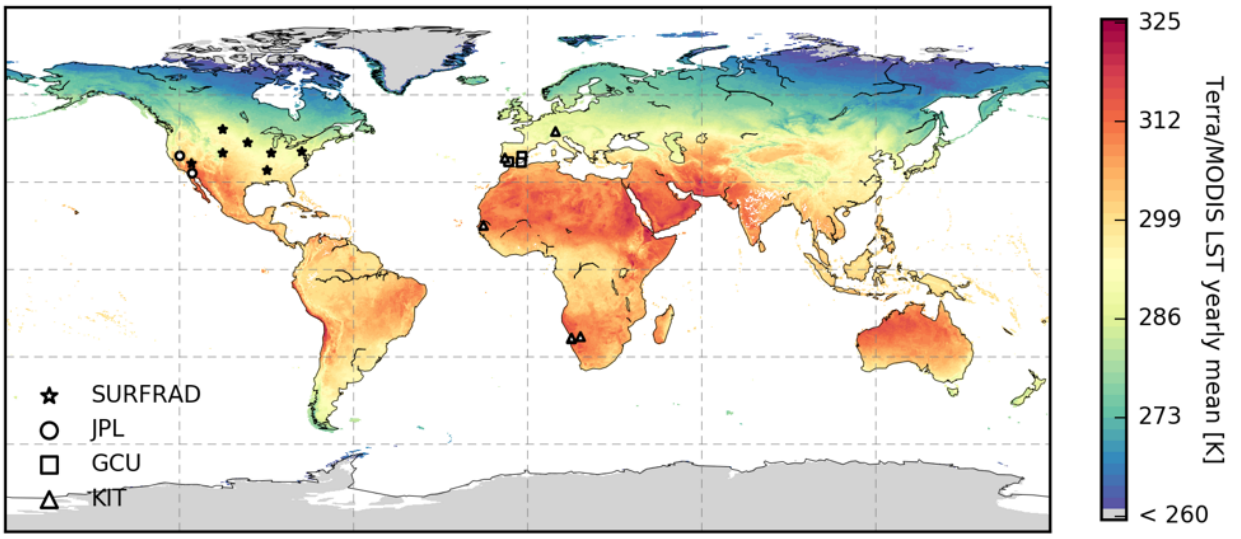

Figure 1. Location of ground observational networks currently used to validate standard LST products derived from US and European spaceborne instruments.

The process of improving both space-based observations and in situ networks is embodied in the GCOS Implementation Plans and the accompanying Satellite Supplements (GCOS-200). The Committee on Earth Observation Satellites (CEOS) Working Group on Calibration and Validation (WGCV), and in particular its subgroup on Land Product Validation (LPV), plays a key coordination role and lends the expertise required to address actions related to the validation of LST measurements as follows:

- In-situ LST is usually estimated from up- and downwelling thermal infrared (TIR) radiance measurements near the surface. The radiances are either obtained with a set of radiometers (directional measurements) or pyrgeometers (hemispherical measurements). A number of observational sites dedicated to surface climate, ecological, or agricultural research and applications provide in-situ LST on a routine basis. CEOS WGCV plays a coordinating role in this work. Benchmarking and consistency checking are required for the global archive of LST observations.
- The setting up and maintenance of reference sites to address the inadequate or missing reference network need to be undertaken. Building on existing networks - such as the National Oceanic and Atmospheric Administration (NOAA) Surface Radiation (SURFRAD) and US Climate Reference Network (CRN) networks, the Land Surface Analysis – Satellite Application Facility (LSA–SAF) permanent validation sites for EUMETSAT satellite products, NASA's Jet Propulsion Laboratory (JPL) validation sites - is the most promising way to improve this situation.
- Benchmarking and comparison of satellite-derived LST products is essential to resolve differences between products and to ensure their consistency in terms of accuracy and reliability. The CEOS WGCV is leading this activity in collaboration with GCOS and TOPC, exploiting in situ observations from designated reference sites and building on the validation activities currently being undertaken by the space agencies and associated research programs (GCOS-200, p. 203).

CEOS considers these roles important to achieving validated global LST products, but at the same

time, recognizes current limitations in both resources and knowledge within both CEOS and the international expert community. This good practice document includes recommendations from CEOS that, if followed, should serve to remove many of the current limitations.

1.4 LST Requirements

The user-driven baseline requirements for satellite-derived LST climate data records (Table 1) used in climate studies have been determined by the CEOS WGCV Land Product Validation subgroup and the International Land Surface Temperature and Emissivity Working Group (http://ilste-wg.org). The values in Table 1 are the thresholds that represent the minimum requirements for LST data to be useful for climate applications (GCOS-200); target values are indicated where understood (i.e. length of record requirements are difficult to quantify). In this protocol, we will focus primarily on LST datasets generated from infrared instruments, which only allow LST retrievals under clear sky conditions. Although LST can also be estimated from passive micro-wave sensors under both clear and cloudy situations (e.g., Jimenez *et al.*, 2017), micro-wave based LST are not only beyond the spatial resolution threshold (Table 1), as their maturity has not yet reached that of infrared based products (e.g., Ermida *et al.*, 2017).

Table 1. LST product requirements for climate related studies

Requirement	**Threshold**	**Target (breakthrough)**
Horizontal resolution	5 km (i.e. 0.05°)	≤ 1 km
Temporal resolution	≤ day/night (12h)	3-hourly
Uncertainty	1 K	0.1 K
Precision	1 K	0.1 K
Stability	≤ 0.3 K per decade	≤ 0.1 K per decade
Length of record	20 years	>30 years

It should be noted that LST product requirements strongly depend on the target application. For example, agricultural applications such as crop condition monitoring or irrigation management, require higher spatial resolutions (~100 m or higher).

1.5 Rationale for Requirements for Climate Applications

LST is the intrinsic quantity required by the climate user community. However, it is recommended that emissivity values are reported as part of a climate quality LST product. Likewise, although sensor and channel specific, it is recommended that land surface brightness temperature is also reported as part of the LST climate quality product to allow producers and users to derive LST data sets with alternative retrieval methods.

Although there are issues with respect to satellite radiometer stability and cloud masks reliability, the specifications of existing (and planned) space-based instruments meet or largely exceed the spatial and temporal sampling requirements of General Circulation Models (GCM). The higher frequency of observations today provide us with accurate and stable products that are able to support a host of other downstream applications. Even in the context of climate applications, high spatial resolution products support high-resolution regional models, as well as global models, and allows for examination of the sensitivity of land-surface parameterizations with respect to surface heterogeneity, and to capture rapid

changes in vegetation phenology, surface hydrology, and anthropogenic effects.

1.6 Goal of this Document

The goal of this document is to identify and promote good practices for the validation of global satellite LST products. The document specifically addresses uncertainty assessment against reference datasets. The latter should be traceable to in situ measurements of known accuracy, and the assessment augmented with metrics of precision derived from ensembles of products themselves. The development of validation protocols also addresses the GCOS Action Items.

2 DEFINITIONS

This section provides the necessary definitions relevant to global LST validation.

2.1 Definition of Land Surface Temperature

LST is a kinetic quantity, independent of wavelength, that represents the thermodynamic temperature of the skin layer of a given surface, i.e. a measure of how hot or cold the surface of the Earth would feel to the touch. For ground-based, airborne, and spaceborne remote sensing instruments LST is the aggregated radiometric surface temperature, i.e. based on a measure of radiance (Norman and Becker, 1995), of the ensemble of components within the sensor field of view. LST is sometimes referred to in the literature as (directional) radiometric temperature or skin temperature. The unit of LST is Kelvin [K]; Degree Celsius [°C] is also commonly used. When derived from radiometric measurements of ground-based, airborne, and space-borne remote sensing instruments, LST is the aggregated radiometric surface temperature of the ensemble of components within the sensor field of view. This definition was adopted across various international groups (CEOS WGCV, GCOS, ESA GlobTemperature, ILSTE-WG), and was pioneered by the work of John Norman and François Becker (see Norman and Becker, 1995, for example).

2.2 Definitions of Associated Physical Parameters

2.2.1 Black body

A black body is an idealized physical body that absorbs all incident electromagnetic radiation in the thermal infrared and does not reflect any. The emissivity of a black body is equal to 1.

2.2.2 Surface emissivity

"Surface emissivity of an isothermal, homogeneous body is defined as the ratio of the actual emitted radiance to the radiance which would be emitted from a perfectly emitting surface (i.e. 'blackbody') at the same thermodynamic temperature" (Norman and Becker, 1995).

2.2.3 Brightness temperature

"Brightness temperature is a directional temperature obtained by equating the measured radiance with the integral over wavelength of the Planck's Black Body function times the sensor response. It is the temperature of a black body that would have the same radiance as the radiance actually observed with the radiometer. This requires specification of wavelength interval, direction and whether the observation is

above the atmosphere from a satellite or immediately above the surface." (Norman and Becker, 1995)

2.3 Definition of Spatial and Geometrical Aspects

Validation of satellite LST products relies on terminology specific to satellite measurements. This section reviews the terminology used in this context. The following definitions were adapted from the Global Leaf Area Index validation best practice document (Fernandes *et al.*, 2014).

2.3.1 Elementary Sampling Unit (ESU)

An Elementary Sampling Unit (ESU) is a contiguous spatial region over which the expected value of LST can be estimated through in situ measurements. The ESU corresponds to the finest spatial scale of LST estimates used for reference. ESU size is bounded by an instrument's sampling characteristics and may involve a number of measurements. Maximum ESU size is determined by the level of within-ESU variability that can be tolerated by the validation protocol. Within a reference region, the appropriate ESU size varies with surface conditions, the instrument used, illumination conditions and spatial sampling design. ESU size should be sufficient to allow repeat visits with negligible uncertainty contributions due to changes in illumination or geolocation.

2.3.2 Local Horizontal Datum

The local horizontal datum is the plane containing the tangent to the local geoid corresponding to the center of an ESU or mapping unit. Depending on the survey method over sloped terrain, corrections of LST estimates for the dependency of observed surface area on slope may be required.

2.3.3 Projected Instantaneous Field of View (PIFOV) of Measurement

The ground projected instantaneous field of view (PIFOV) is the area on the ground corresponding to the region over which a measurement is performed. For radiometric measurements, this area is defined as the region where the instrument point spread function, including all processing aspects except for spatial resampling, exceeds a specified threshold. The majority of imaging scanners including satellite imagers have PIFOV on flat ground on the order of twice the inter pixel sampling distance. The PIFOV of an in situ instrument will vary with the height and angular sampling of the instrument.

2.3.4 Effective Projected Instantaneous Field of View (EPIFOV) of Measurement

The effective projected instantaneous field of view (EPIFOV) corresponds to the PIFOV extended by the impact of spatial resampling. Resampling with smoothing filters (e.g. cubic convolution) will result in an EPIFOV with a size approximating the PIFOV convolved with the size of the filter spatial support. Non-linear resampling, such as nearest neighbor, can result in substantial spatial aliasing. Hence, comparisons of values recorded in different EPIFOVs should include spatial averaging using a filter with a spatial support of several PIFOVs.

2.3.5 Satellite Measurement Geolocation Uncertainty

Geolocation uncertainty corresponds to the planimetric uncertainty of a satellite measurement located on the same projection and datum as the ESU or study site reference LST estimates. Geolocation

uncertainty is often reported in nominal terms and based on a normal distribution of errors. Acquisition specific biases are surprisingly frequent and, therefore, geolocation uncertainty should be visually compared to reference vector layers whenever possible.

2.3.6 Mapping Unit

A mapping unit is the spatial region on the Earth's surface corresponding to a product value for a specified temporal extent. Satellite based LST products represent swaths or gridded digital layers in a specified map projection rather than per nominal EPIFOV location. As such, these products include a spatial generalization corresponding to the transformation of LST estimate over each EPIFOV to the LST estimate for the mapping unit. Considering that GCOS requires gridded LST products at a constant spatial resolution, the CEOS LST validation protocol assumes uncertainties due to this generalization or due to temporal aggregation, are included in total product uncertainty.

2.4 Definition of Validation Metrics

Validation is the process of assessing, by independent means, the quality of the data products derived from those system outputs. In general, the result of a measurement is only an approximation or estimate of the value of the measurand and thus is complete only when accompanied by a statement of the uncertainty of that estimate. Definitions of validation metrics (uncertainty, bias, precision and completeness) drawn from experimental statistics that are applicable to LST are from the Joint Committee for Guides in Metrology (JCGM) guide to the expression of uncertainty in measurement, referred to as GUM-2008 hereafter. The definitions used in this document and reported below are mainly from GUM-2008:

- **Error** (of measurement) is "the result of a measurement minus a true value of the measurand". The true value (of a quantity) is the "value consistent with the definition of a given particular quantity". Since a true value cannot be usually determined, in practice a conventional true value is used. The conventional true value (of a quantity) is the "value attributed to a particular quantity and accepted, sometimes by convention, as having an uncertainty appropriate for a given purpose". Traditionally, an error is viewed as having two components, namely, a random component and a systematic component. The random error is the "result of a measurement minus the mean that would result from an infinite number of measurements of the same measurand carried out under repeatability conditions" and the systematic error is the "mean that would result from an infinite number of measurements of the same measurand carried out under repeatability conditions minus a true value of the measurand".
- **Uncertainty** is a "parameter, associated with the result of a measurement, that characterizes the dispersion of the values that could reasonably be attributed to the measurand". Uncertainty includes bias and precision errors and can be estimated by the Root Mean Square Error (RMSE).
- **Accuracy** is the degree of "closeness of the agreement between the result of a measurement and a true value of the measurand". Commonly, accuracy is represented as a description of systematic errors and a measure of statistical bias. **Bias** is the systematic error between LST products and their reference estimates, i.e. it describes the average deviation from the reference, which is given by the average difference between the LST product and its reference estimate.
- **Precision** or **repeatability** (of results of measurements) is the "closeness of the agreement between the

results of successive measurements of the same measurand carried out under the same conditions of measurement". Commonly, precision represents the dispersion of product retrievals around their expected value and can be estimated by the standard deviation (STD) of the difference between retrieved LSTs and the corresponding reference estimates.

- **Completeness** is the proportion of valid retrievals over an observation domain.

It should be noted that strong and/or multiple outliers affect the classical metrics described above (i.e. mean and STD): in such cases using the median in lieu of the mean to estimate systematic error and the median absolute deviation as a measure of precision is more suitable and should be included in the validation effort.

3 GENERAL CONSIDERATIONS FOR SATELLITE LST PRODUCTS

3.1 Radiance components and LST retrieval

Under clear sky conditions, the top of atmosphere radiance measured by a spaceborne sensor ($L_{sat,\lambda}$) includes contributions from the surface emission, the atmospheric upwelling radiance ($L^{\uparrow}_{sky,\lambda}$) and atmospheric downwelling radiance ($L^{\downarrow}_{sky,\lambda}$) reflected by the Earth's surface and attenuated by the atmosphere (Eq. 1). Retrieval algorithms rely on one or more top-of-atmosphere spectral measurements to account for atmospheric effects and estimate LST.

$$L_{sat,\lambda} = \left[\varepsilon_\lambda B_\lambda(LST) + (1 - \varepsilon_\lambda) L^{\downarrow}_{sky,\lambda}\right] \tau_\lambda + L^{\uparrow}_{sky,\lambda} \quad (1)$$

where ε_λ is the spectral emissivity at wavelength λ or representative of a specific (relatively narrow) domain [λ_1, λ_2] centered on wavelength λ, $B_\lambda(T)$ is the Planck function describing the radiance of a black body at temperature T, and τ_λ is the atmospheric transmittance.

3.2 Current satellite-based LST products

Operational LST products are currently available from a variety of instruments. In this document, we mainly focused on products that can be used for climate related studies (i.e. following product requirements described in Table 1). We have selected some of most commonly used operational and standard LST products to present the different retrieval algorithms that can be used at moderate resolution, and present the potential sources of uncertainty that have been already discussed in the literature. The selected products are based on radiometric measurements by the Moderate Resolution Imaging Spectroradiometer (MODIS) sensor aboard the Terra and Aqua satellites, the Advanced Baseline Imager (ABI) aboard Geostationary Operational Environmental Satellite (GOES)-R, the Spinning Enhanced Visible & Infrared Imager (SEVIRI) aboard the Meteosat satellite series, the Sea and Land Surface Temperature Radiometer (SLSTR) on the Sentinel-3 platform and the Visible Infrared Imaging Radiometer Suite (VIIRS) onboard the S-NPP satellite.

3.2.1 MODIS

3.2.1.1 Split-window-based algorithm

NASA's operational MODIS LST product based on the split-window approach consists of Level-2 (MOD11_L2) products at the spatial resolution of MODIS, i.e. 927 m at nadir, and gridded Level-3 (MOD11A1, MOD11A2, MOD11B1, MOD11C1, MOD11C2, MOD11C3) products at 1km or 5km spatial resolution. Satellite overpass times at the equator are around 10:30am/pm (local solar time) for Terra and 1:30am/pm for Aqua. Along each scan, the MODIS off-nadir scan angle increases to values of up to 65°, which causes the sensor's spatial resolution to degrade to about 6 km in the along-scan direction. The generalized split-window algorithm (Wan and Dozier, 1996) is used to derive LST values from brightness temperature measurements in MODIS band 31 (T_{31}) and band 32 (T_{32}) centered on 11.03 µm and 12.02 µm, respectively (Eq. 2).

$$LST = b_0 + \left(b_1 + b_2\frac{1-\varepsilon}{\varepsilon} + b_3\frac{\Delta\varepsilon}{\varepsilon^2}\right)\frac{T_{31}+T_{32}}{2} + \left(b_4 + b_5\frac{1-\varepsilon}{\varepsilon} + b_6\frac{\Delta\varepsilon}{\varepsilon^2}\right)\frac{T_{31}-T_{32}}{2} \qquad (2)$$

where ε and $\Delta\varepsilon$ are the mean and the difference of the emissivity values in bands 31 and 32. The algorithm coefficients b_k (with k = 0 to 6) depend on viewing zenith angle, surface air temperature (T_{air}) and atmospheric water vapor content. The coefficients were derived for daytime and nighttime from regression analysis of radiative transfer simulation data for a comprehensive set of LST values varying from T_{air} – 16 K to T_{air} + 16 K (Wan and Dozier, 1996) accounting for the MODIS spectral response function - see Figure 2. In the standard LST product, information about surface air temperature and total column water vapor is taken from the MODIS atmospheric profile product (MOD07) (Wan, 2008). For each surface type, the spectral emissivity values in band 31 and 32 (Eq. 1) are defined as a combination of green and senescent components (Snyder *et al.*, 1998).

3.2.1.2 Temperature Emissivity Separation (TES) algorithm

Initially developed for the Advanced Spaceborne Thermal Emission and Reflection Radiometer (ASTER) sensor on Terra, the Temperature-Emissivity Separation (TES) method (Gillespie *et al.* 1998) is an alternative physics-based approach that was adapted for MODIS (Hulley and Hook, 2010) in order to address emissivity related issues in the heritage MOD11 products resulting in underestimation of LST in arid regions (Gottsche and Hulley 2012; Hulley and Hook 2009; Malakar and Hulley 2016). The new TES-based product, termed MOD21 includes both LST and physically retrieved emissivity for the 3 MODIS thermal bands (29, 31, 32) and is currently being produced as part of the MODIS Collection 6 suite of products. The TES algorithm uses a radiative transfer model to correct at-sensor radiances to surface radiances and a statistical emissivity model to separate contributions from surface temperature and emissivity. The approach requires atmospheric profiles from either satellite sounding or conventional radiosondes and an emissivity model which is typically based on laboratory and field measurements (Kealy and Hook, 1993; Matsunaga, 1994). In the TES approach, first the range of relative spectral emissivities (i.e. the minimum-maximum difference or MMD) is calculated. A calibration curve derived from laboratory data (Matsunaga, 1994) allows to estimate minimum absolute spectral emissivity from the observed MMD value. Equation 1 is then used to compute LST and emissivities for the other bands. For MODIS, the ASTER

spectral library (Baldridge *et al.*, 2009) is used to derive the calibration curve for three TIR bands: 29 (8.55 µm), 31 (11 µm) and 32 (12 µm): the regression between the minimum emissivities and MMDs obtained for MODIS is given by Equation 3.

$$\epsilon_{min} = 0.985 - 0.7503\, MMD^{0.8321} \quad (3)$$

where, ε_{min} is the minimum emissivity of the three MODIS TIR bands (29, 31 and 32), and MMD is the difference between the minimum and maximum emissivity values for the given bands. The TES algorithm is combined with an improved Water Vapor Scaling (WVS; Tonooka, 2005) atmospheric correction scheme to adjust the retrieval during very warm and humid conditions. Validation results have shown consistent accuracies at the 1 K level over all land surface types.

3.2.2 SEVIRI

EUMETSAT's operational LST product for SEVIRI is produced by the Satellite Applications Facility on Land Surface Analysis (LSA SAF). It is computed every 15 minutes at a spatial resolution of 3 km (sampling distance at nadir) within the area covered by the Meteosat Second Generation (MSG), i.e. primarily over Europe, Africa and South America. The retrieval is based on the Generalized Split-Window algorithm (GSW; Wan and Dozier, 1996; Eq. 2) and uses brightness temperatures measured in channels 9 and 10 centered on 10.8 µm and 12.0 µm, respectively. Emissivity is obtained with the so-called vegetation cover method (Caselles and Sobrino, 1989; Peres and DaCamara, 2005), where effective channel emissivity for any given pixel is estimated as a weighted average of channel emissivities of the dominant bare ground and vegetation types within a scene. The emissivity values for these types are available from look-up tables (Peres and DaCamara, 2005) determined for International Geosphere-Biosphere Program (IGBP) land cover classes (Belward, 1996). Actual channel emissivities are then estimated from the fraction of vegetation cover (FVC) also retrieved by LSA SAF (Garcia-Haro *et al.*, 2005) as five-day composites updated on a daily basis. Furthermore, the GSW parameters are selected based on forecasts of total column water vapour provided by the European Centre for Medium-range Weather Forecasts (ECMWF). LSA SAF performed an in-depth analysis of the various error sources of its GSW algorithm and utilises these to maximize the LST product's spatial coverage (Freitas *et al.*, 2010). The LST values are distributed together with realistic estimations of the respective uncertainties on a pixel-by-pixel basis, allowing users to decide if specific LST data meet their application requirements. The target accuracy of the SEVIRI LST product is 2 K (Freitas *et al.*, 2010), while validation against in-situ data showed a general uncertainty of about 1.5 K (Göttsche *et al.*, 2016). The LSA SAF LST product is described in detail in the corresponding Algorithm Theoretical Basis Document (Trigo *et al.*, 2009).

3.2.3 VIIRS

Since August 11, 2012, the NOAA VIIRS Environmental Data Record (EDR) has been operationally produced using a single split window algorithm (Yu *et al.*, 2005). The algorithm uses brightness temperatures measured in channel M15 (T_{15}) and channel M16 (T_{16}) centered on 10.76 µm and 12.01 µm, respectively (Eq. 4).

$$LST = a_0 + a_1\, T_{15} + a_2\, (T_{15} - T_{16}) + a_3\, (sec\theta_v - 1) + a_4\, (T_{15} - T_{16})^2 \quad (4)$$

where a_k (with k = 0 to 4) are the algorithm coefficients and θ_v is the sensor zenith angle. Daytime and nighttime sets of coefficients were derived for 17 different surface types from regression analysis of MODTRAN radiative transfer simulations for globally representative atmospheric and surface conditions (VIIRS LST Algorithm Theoretical Basis Document (ATBD), 2011). The International Geosphere-Biosphere Programme (IGBP) global classification map is used to identify the surface type associated with each pixel. The algorithm regression coefficients were generated from an ensemble of MODTRAN radiative transfer simulations using a comprehensive set of geophysical parameters (VIIRS LST ATBD, NOAA 2011). Surface temperatures and coherent atmospheric temperature and water vapor profiles were derived from National Center for Environmental Prediction (NCEP) global simulations at 2.5° x 2.5° spatial resolution. LST values were sampled from 196 K to 327 K. Distribution of band-averaged spectral emissivity values for each surface type (Eq. 1) were derived from the MOSART database (VIIRS LST ATBD, NOAA, 2011). These were used to produce a total of 268,128 samples representing 12 days and nights (one day and night per month) over a global grid, and provided an ensemble of training data covering global, diurnal and seasonal features (VIIRS LST ATBD, 2011). The spatial resolution of VIIRS raw radiometric measurements at moderate resolution is around 750 m at nadir and around 1.5 km at the edge of the swath. VIIRS detectors are rectangular, with the smaller dimension projecting along the scan. At nadir, three detector footprints are aggregated to form a single VIIRS pixel. Moving along the scan away from nadir, the detector footprints become larger both along track and along scan, due to geometric effects and the curvature of the Earth (Wolfe *et al.*, 2013). The pixel aggregation scheme is changed from 3 to 2 detectors at a scan angle of around 32°, and from 2 to 1 detector at around 48°, which provides a more uniform pixel size over the scan. The bias and precision requirements specified by NOAA's Joint Polar Satellite System (JPSS) program for the VIIRS LST EDR are 1.5 K and 2.5 K, respectively, for clear conditions.

In line with production of the new MOD21 LST&E product, NASA is currently in the processing of producing an equivalent TES-based product for VIIRS, termed VNP21. The VIIRS Land Surface Temperature and Emissivity (LST&E) algorithm and data products (VNP21) in Collection 1 (C1) are being developed synergistically with the MODIS Collection 6 (C6) LST&E algorithms and data products (MOD21) using the same algorithmic approach and input atmospheric products (Islam *et al.*, 2016; Malakar and Hulley, 2016).

3.2.4 NOAA Enterprise LST algorithm

NOAA JPSS Land EDR team is developing an enterprise LST algorithm that will be used for both the JPSS and GOES-R satellite missions. The enterprise algorithm is based on the split-window approach, using spectral measurements at channels centered on 11 and 12 μm, respectively, and spectral emissivity data (Eq. 5).

$$LST = C_0 + C_1 T_{11} + C_2 (T_{11} - T_{12}) + C_3 \varepsilon + C_4 \varepsilon (T_{11} - T_{12}) + C_5 \Delta\varepsilon \quad (5)$$

where C_i, i=0 to 5, are the algorithm coefficients; T_{11} and T_{12} are the brightness temperatures measured at the split-window channels (i.e. 11 μm and 12 μm), respectively; ε and $\Delta\varepsilon$ are the mean emissivity and the spectral emissivity difference, respectively. Note that the different coefficients set {C_i} are estimated for daytime and nighttime, and for different atmospheric water vapor conditions. Coefficients are calculated for

the JPSS satellite sensor (i.e. VIIRS) and for the GOES-R sensor (i.e. Advanced Baseline Imager, ABI) accounting for differences in the sensor spectral response function. The split window channels are bands M31 and M32 for VIIRS, and bands M15 and M16 for ABI.

3.2.5 SLSTR

ESA's Sentinel-3A SLSTR instrument, launched in February 2016, provides MODIS/VIIRS-like data (Fig. 2), with a 10am overpass. The SLSTR algorithm (Eq. 6) is an evolution of the LST algorithm developed for the Advanced Along Track Radiometer (AATSR), aboard ENVISAT, by Prata (2002).

$$LST = a_{f,i,w} + b_{f,i}(T_{11} - T_{12})^n + \left(b_{f,i} + c_{f,i}\right)T_{12} \tag{6}$$

with $$n = 1/\cos\left(\frac{\theta_v}{m}\right),\quad a_{f,i,w} = d(sec\theta_v - 1)pw + a_{v,i}f + a_{s,i}(1-f),$$
$$b_{f,i} = b_{v,i}f + b_{s,i}(1-f) \quad \text{and} \quad c_{f,i} = c_{v,i}f + c_{s,i}(1-f)$$

where T_{11} and T_{12} are the brightness temperatures from the SLSTR 11 µm and 12 µm bands respectively, θ_v is the satellite view zenith angle, f is the vegetation fraction, w is the atmospheric water content (in cm) and i corresponds to the surface type or biome from the Globcover classification. $a_{v,i}$, $a_{s,i}$, $b_{v,i}$, $b_{s,i}$, $c_{v,i}$ and $c_{s,i}$ represent the algorithm regression coefficients derived for each of the 22 biomes of Globcover (i) calculated for a vegetation cover fraction of 100% (v) and for a bare soil (s). Two sets of coefficients are derived for daytime and nighttime observations accounting for the SLSTR spectral response functions (Figure 2). d and m are two empirical parameters. A full description of the retrieval algorithm can be found in the SLSTR Algorithm Theoretical Basis Document (ATBD) for Land Surface Temperature (Remedios, 2012).

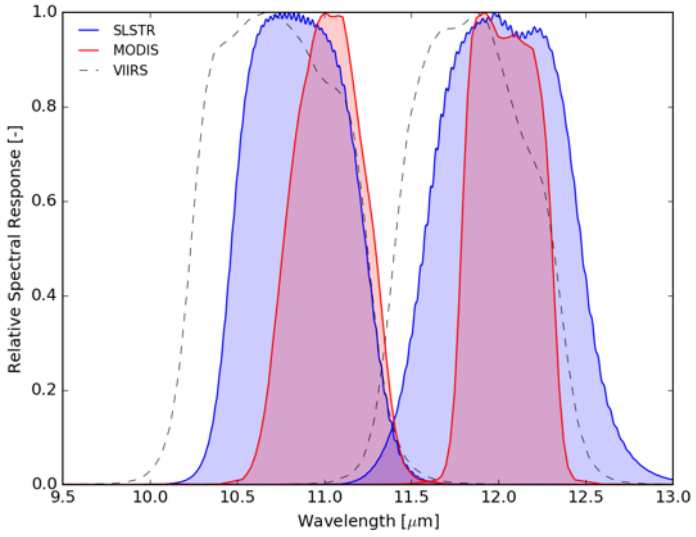

Figure 2: Relative spectral response of the SLSTR, MODIS and VIIRS thermal bands around 11 µm and 12 µm. Data are from the MODIS Characterization Support Team at NASA Goddard Space Flight Center for MODIS, from NOAA National Calibration Center for VIIRS and from ESA Sentinels Scientific Data Hub for SLSTR.

3.3 GENERAL CONSIDERATIONS FOR IN SITU REFERENCES

From *in situ* narrow band measurements of surface-leaving radiance $L_{ground,\lambda}$ and downwelling radiance from the sky $L^{\downarrow}_{sky,\lambda}$ ground-based LST (LST_{ground}) is retrieved using Planck's law (Guillevic *et al.*, 2014; Göttsche *et al.*, 2016) (Eq. 7).

$$LST_{ground} = B_{\lambda}^{-1}\left[\frac{1}{\varepsilon_{\lambda}}\left(L_{ground,\lambda} - (1-\varepsilon_{\lambda})L^{\downarrow}_{sky,\lambda}\right)\right] \quad (7)$$

where ε_{λ} is the spectral emissivity at wavelength λ or representative of a specific (relatively narrow) domain [λ_1, λ_2] centered on wavelength λ, $B_{\lambda}(T)$ is the Planck function describing the radiance of a black body at temperature *T*.

In contrast, from broadband radiance measurements L_{ground} and $L^{\downarrow}_{sky}$, LST_{ground} is retrieved using Stefan-Boltzmann's law (Eq. 8) (Wang and Liang, 2009):

$$LST_{ground} = \left[\frac{1}{\varepsilon\sigma}\left(L_{ground} - (1-\varepsilon)L^{\downarrow}_{sky}\right)\right]^{1/4} \quad (8)$$

where ε is the broadband emissivity and σ the Stefan-Boltzmann constant (=5.67 10^{-8} $Wm^{-2}K^{-4}$). Broadband emissivity can be retrieved from 'narrowband' satellite emissivities (e.g. MODIS) via empirical relationships (Wang and Liang, 2009). Furthermore, empirical relationships can be obtained to map emissivities from one satellite sensor to another, e.g. from MODIS to SEVIRI (Peres *et al.*, 2014).

For information on determining in-situ LST and emissivity please refer to Appendix B, which provides relevant details and best practices from (Göttsche et al., 2017).

3.3.1 Existing in situ networks of LST reference measurements

Several networks and dedicated validation stations are commonly used to validate current standard and research LST products, e.g. NOAA's Surface Radiation (SURFRAD) network, the US Climate Reference Network (CRN), KIT's permanent validations stations operated within the framework of EUMETSAT's Land Surface Analysis Satellite Application Facility (LSA SAF), the NASA JPL validation sites, the Fluxnet tower network, and the sites of the Global Change Unit (GCU) of the University of Valencia in Spain. These existing observational networks (Table 2) include appropriate tower sites with appropriate sensors and support (e.g. human maintenance, radiometer availability, site accessibility, and power needs) required for measuring radiation variables to derive LST. A challenge in deriving high quality in-situ LST is to estimate critical ancillary data, such as surface emissivity and atmospheric profiles if downwelling atmospheric radiance is not simultaneously measured. Usually, ancillary data are not routinely collected and have to be obtained from other sources. While surface measurements are too sparse to systematically validate remote sensing products in a global sense, they are the only means to validate LST products in a classical sense, i.e. with independent measurements, and they complement scientific efforts aimed at comparing and benchmarking the various existing LST products. Pursuing and expanding these measurements is essential to ensure the quality and reliability of current and future products, to provide a step towards more accurate and consistent LST information for the global landmass and to serve further development of associated

standards. However, the largest networks (i.e. Fluxnet, SURFRAD and US CRN) were not specifically set up for LST product validation and the stations are frequently located in heterogeneous areas, resulting in observations that are not representative of spatially coarser satellite observations. For such sites, validation with ground-based LST should be limited to night-time when land surfaces tend to be close to isothermal (Wang *et al.*, 2008; Guillevic *et al.*, 2014; Martin and Göttsche, 2016).

Table 2. In-situ LST networks.

Name	Type	Land Cover	Citation
FLUXNET	Hemispherical pyrgeometers	All surface types	
JPL network	Radiometers	Water bodies, agricultural field	Hook *et al.*, 2007
SURFRAD	Hemispherical pyrgeometers	Short vegetation and barren soils in the USA	Augustine *et al.*, 2000, 2005
US CRN	Radiometers	Short vegetation and barren soils in the USA	Diamond *et al.*, 2013
GCU stations	Radiometers	Various surface types in Spain	Sobrino and Skokovic, 2016
KIT stations	Radiometers	Various surface types in Africa and Portugal	Göttsche *et al.*, 2016

Links to all ground-based LST measurement protocols can be found at the LPV sub-group Surface LST&E Focus Area webpage (https://lpvs.gsfc.nasa.gov/LST_home.html).

3.3.1.1 Fluxnet network

The Fluxnet network (Baldocchi *et al.*, 2001) provides continuous observations of ecosystem level exchanges of CO2, water and energy, and micrometeorological parameters at diurnal, seasonal, and interannual time scales. The FLUXNET stations operate in climatologically diverse regions and are representative of various land cover types (Table 3). Over the contiguous United States, the Fluxnet stations are part of the Ameriflux network and collect measurements of radiative forcing (shortwave and longwave downwelling and outgoing radiation), surface fluxes (soil heat and convective fluxes), and atmospheric parameters (air temperature and wind speed). AmeriFlux instruments are meticulously maintained and a detailed description of the network and a summary of the accuracy assessment of each instrument are provided by Baldocchi *et al.* (2001). Upwelling and downwelling thermal infrared radiances measured by two pyrgeometers (spectral range from around 3.5 to 50.0 μm) can be used to derive ground-based LST following Equation 7. However, despite the good quality of the collected data, the FLUXNET network has not been used for satellite-derived LST product validation in a routine manner yet. AmeriFlux data are archived and distributed by the Oak Ridge National Laboratory (http://ameriflux.ornl.gov/). For each selected site, the dataset represents 30-minute averages of each parameter.

Table 3. Examples of FLUXNET/AmeriFlux stations including site geolocation, primary surface type and available period of time for each dataset

Site	Lat	Lon	Surface type	Period	Climate
ARM Great Plains, OK	36.606	-97.489	Cropland	2003-2012	Temperate
Audubon Ranch, AZ	31.591	-110.509	Grassland	2004-2008	Semi-arid
Bondville, IL	40.006	-88.290	Cropland	1997-2007	Temperate

Brookings, SD	44.345	-96.836	Grassland	2005-2009	Temperate
Chestnut Ridge, TN	35.931	-84.332	Deciduous broadleaf	2006-2013	Temperate
Fermi, IL - Agricultural	41.859	-88.223	Cropland	2006-2011	Temperate
Fermi, IL - Prairie	41.841	-88.241	Grassland	2005-2011	Temperate
Fort Peck, MT	48.308	-105.102	Grassland	2000-2008	Temperate
Freeman Ranch, TX - Mesquite	29.950	-97.996	Grassland	2005-2008	Semi-arid
Freeman Ranch, TX - Woodland	29.940	-97.990	Woody savannah	2005-2012	Semi-arid
Konza, KS	39.082	-96.560	Grassland	2007-2012	Temperate
Loblolly Pine, NC	35.803	-76.668	Evergreen needleleaf	2005-2010	Sub-tropical
Loblolly Pine Clearcut, NC	35.812	-76.712	Evergreen needleleaf	2005-2009	Sub-tropical
Mead, NE - Irrigated maize	41.165	-96.477	Irrigated cropland	2002-2012	Temperate
Mead, NE - Irrigated maize-soybean	41.165	-96.470	Irrigated cropland	2002-2012	Temperate
Mead, NE - Rainfed maize-soybean	41.180	-96.440	Rainfed cropland	2002-2012	Temperate
Missouri Ozark, MO	38.744	-92.200	Deciduous broadleaf	2005-2013	Temperate
Santa Rita Mesquite, AZ	31.821	-110.866	Woody savannah	2004-2013	Semi-arid
Tonzi Ranch, CA	38.432	-120.966	Woody savannah	2002-2012	Semi-arid
Vaira Ranch, CA	38.413	-120.951	Grassland	2001-2012	Semi-arid
Walker Branch, TN	35.959	-84.287	Deciduous broadleaf	1995-2006	Temperate

3.3.1.2 NASA JPL sites

NASA's Jet Propulsion Laboratory (JPL) has been maintaining continuous LST monitoring stations on Lake Tahoe, CA/NV, a 35 km long and 15 km wide lake on the California – Nevada border since 1999 and on the Salton Sea, CA, an inland saline lake located in the Sonoran Desert, in south-eastern California since 2006 (Table 4). Each station has a JPL-built self-calibrating thermal infrared radiometer that measures surface brightness temperature in the 8-14 µm spectral domain from a height of 1 m and several bulk temperature sensors, placed around 2 cm beneath the surface (Figure 3). The radiometers are typically exchanged at 6-month intervals for maintenance. Validation at JPL's NIST-traceable calibration facility indicates that changes during deployments are less than 0.05 K (Hook *et al.*, 2003). A full meteorological station (wind speed, wind direction, air temperature, relative humidity and net radiation) is also deployed at each station. The temporal resolution of the in-situ measurements is 2 minutes. For product validation purposes (Guillevic *et al.*, 2014 for example), channel-specific (8-14 µm) incoming atmospheric radiation required for atmospheric correction (Eq. 6) are derived from MODTRAN 5.2 simulations using atmospheric profiles obtained from local sounding balloon launches and model data generated by the National Centers for Environmental Prediction (NCEP). NCEP produces global model values on a 1^{o} x 1^{o} grid at 6 hour intervals. Lake Tahoe is on a grid point and the NCEP data are interpolated to the satellite overpass times. More information on the measurements can be found at at https://laketahoe.jpl.nasa.gov and https://saltonsea.jpl.nasa.gov/.

Table 4. List of JPL inland water sites including geolocation, elevation, surface emissivity and basic description of the surface type at station location and around the station within moderate resolution satellite footprints.

Site location	**Latitude**	**Longitude**	**Elevation**	**Surface type at station**	**Surface type around station**	**Surface emissivity**
Lake Tahoe, CA/NV	39.153° N	120.000° W	1897 m	Inland water	Inland water	0.990
Salton Sea, CA	33.225° N	115.824° W	-226 m	Inland water	Inland water	0.990

3.3.1.3 SURFRAD network

The Surface Radiation Budget Network (SURFRAD) was established in 1993 with the primary objective of supporting climate research with accurate, continuous, long-term measurements of the surface radiation budget over the United States in support of the global Baseline Surface Radiation Network (BSRN) (Augustine *et al.*, 2000, 2005). Seven SURFRAD stations are operating in climatologically diverse regions and are representative of various land cover types (Table 5; Figure 3). Quality-controlled measurements of all relevant radiative components (upwelling and downwelling, solar and infrared, solar direct and diffuse, photosynthetically active, UVB), and meteorological parameters are provided by SURFRAD once per minute. SURFRAD instruments are meticulously maintained, and all instruments are replaced on an annual basis with freshly calibrated instruments. The primary measurements needed to derive ground-based LST are the upwelling and downwelling thermal infrared radiances, which are measured by two pyrgeometers (Eppley Precision Infrared Radiometer, spectral range 3.5 to 50.0 µm). The accuracy of the Eppley pyrgeometer is about 4.2 W m^{-2}, and the precision of the instrument is less than 1 W m^{-2} for nighttime measurements and around 2 W m^{-2} for daytime measurements (Philipona *et al.*, 2001). The spatial representativeness of the pyrgeometer measurements is around 70 x 70 m^2. The instrumental error on its own gives rise to an uncertainty in retrieved LST of less than 1 K (Guillevic *et al.*, 2012). Measurements from SURFRAD have been used by Wang *et al.* (2008), Wang and Liang (2009) and Guillevic *et al.* (2012, 2014) for evaluating ASTER, MODIS and VIIRS LST products, for example.

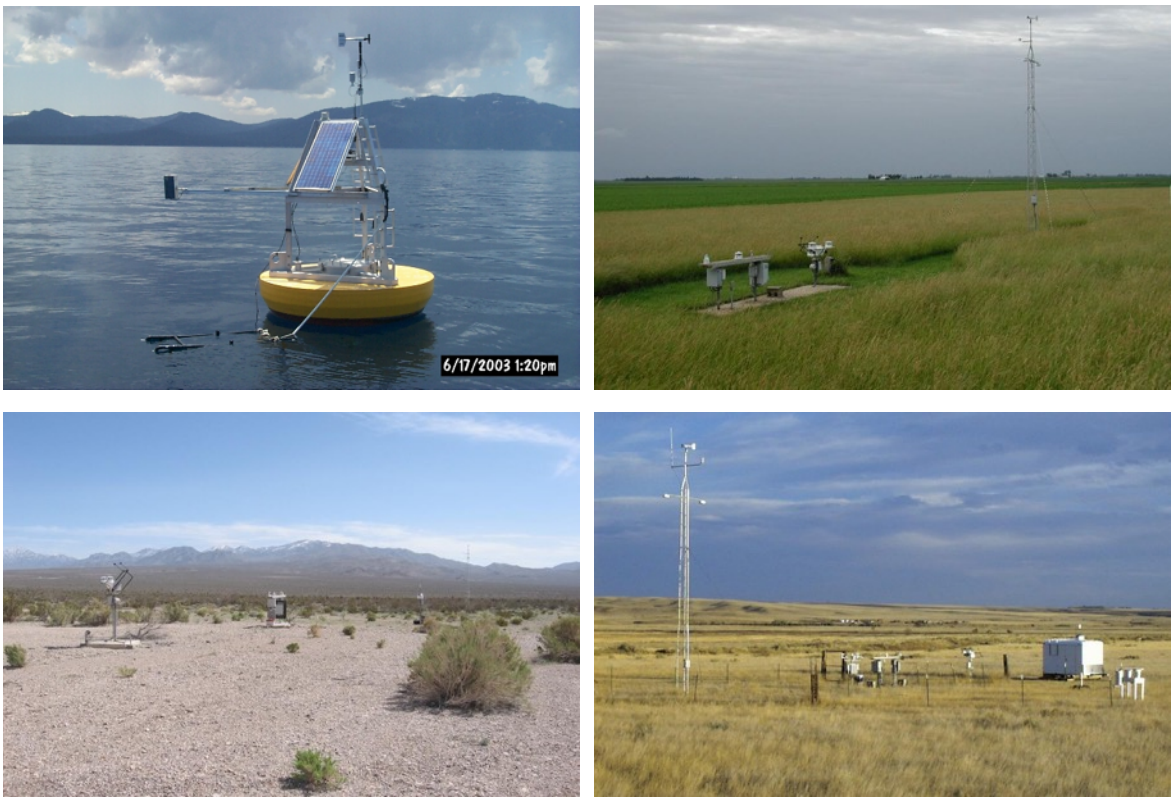

Figure 3. Pictures of four different field stations: instrumented JPL's buoys over Lake Tahoe (upper left), stations from NOAA's SURFRAD network - Bondville, IL (upper right), Desert Rock, NV (bottom left) and Fort Peck, MT (bottom right).

Table 5. List of validation sites including geolocation, elevation, broadband emissivity and basic description of the surface type at station location and around the station within moderate resolution satellite footprints.

Site location	Latitude	Longitude	Elevation	Surface type at station	Surface type around station	Surface emissivity
Table Mountain, CO	40.126° N	105.238° W	1692 m	Sparse grassland	Grassland/crop	0.973
Bondville, IL	40.051° N	88.373° W	213 m	Grassland	Cropland	0.976
Goodwin Creek, MS	34.255° N	89.873° W	96 m	Grassland	Grassland	0.975
Fort Peck, MT	48.308° N	105.102° W	636 m	Grassland	Grassland	0.979
Desert Rock, NV	36.623° N	116.020° W	1004 m	Arid shrubland	Arid shrubland	0.966
Penn State U., PA	40.720° N	77.931° W	373 m	Cropland	Cropland/ forest	0.972
Sioux Falls, SD	43.734° N	96.623° W	483 m	Grassland	Grassland/ urban	0.978

3.3.1.4 NOAA USCRN network

The U.S. Climate Reference Network (USCRN) provides weather and climate measurements from 120 stations developed, deployed, managed, and maintained by NOAA in the continental United States (Fig. 4) for the express purpose of detecting the signal of climate change (Diamond *et al.*, 2013). The USCRN provides stable surface air temperature and relative humidity, precipitation, soil temperature and moisture, solar radiation and surface radiometric temperature observations that are accurate and representative of local environmental conditions (Fig. 5). Station locations have been carefully selected to avoid areas subject to manmade influences (e.g. changing land use and land cover). Accurate climate representativeness and long-term maintenance at each USCRN station location are essential requirements for a climate monitoring network and a long-term validation process.

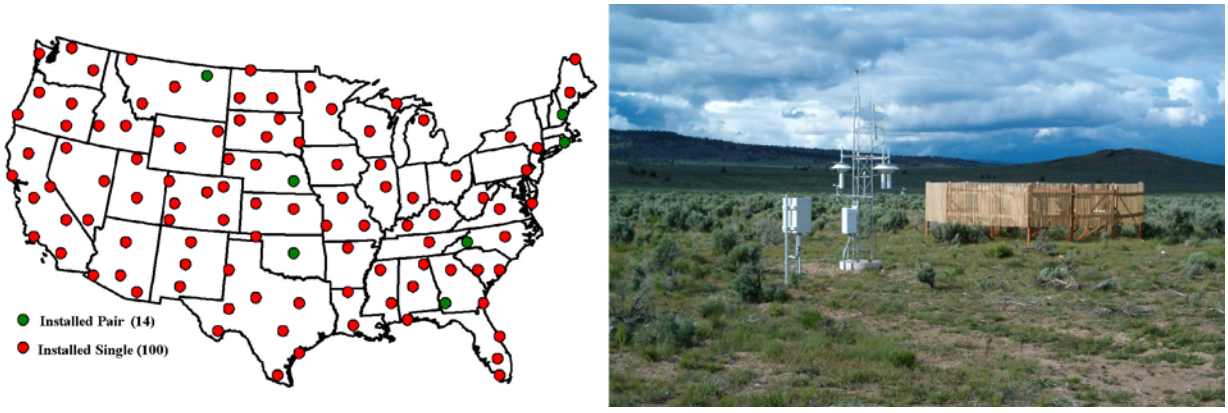

Figure 4. (left) Locations of the U.S. CRN stations over the USA. (Right) Photography of the station located in Riley, OR.

As 5-minute and hourly observations are collected at each USCRN station, three one-hour records of observations are transmitted via GOES satellite telemetry to NCDC every hour. The observations are quickly processed at NOAA's National Centers for Environmental Information (NCEI) to ensure data quality and for computation of official 5-minute and hourly observations from the multi-sensor configuration. This allows the user community to perform near real time product validation.

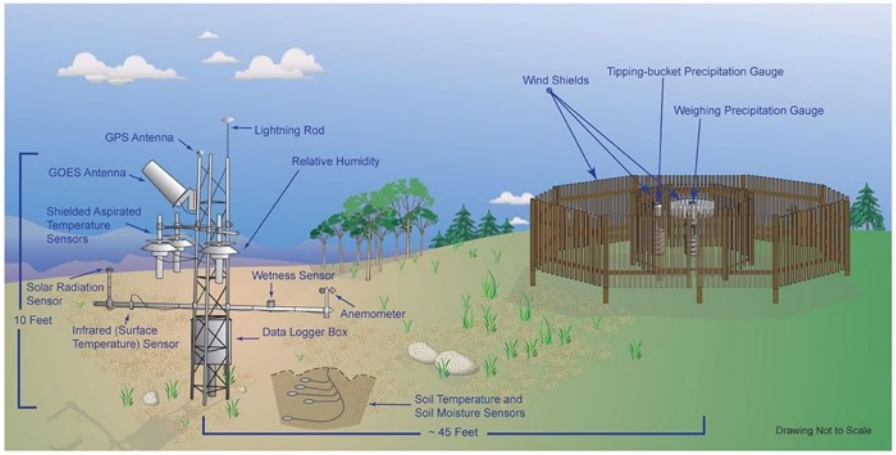

Figure 5. Schematic description of a U.S. Climate reference Network station. Each station has the same design. Courtesy of the NCDC's graphic team.

An Apogee Instruments IRTS-P infrared radiometer measures the surface leaving radiance between 6 to 14 μm, which is converted to brightness temperature. The uncertainty of the sensor is 0.2°C from 15°C to 35°C and 0.3°C from 5°C to 45°C, and the precision is 0.05°C from 15°C to 35°C. The sensor is sampled every two seconds from which 5-minute averages are obtained. The sensor has a 3:1 field of view (FOV), i.e., from 3m height (1.3m), the sensor's circular FOV has a diameter of 1m (0.4m). The IRTS-P is mounted 1.3 meters above the ground near the end of a 3-meter cross-member arm and points vertically downward.

3.3.1.5 GCU stations

In the framework of the CEOS-Spain project, the Global Change Unit (GCU) of the University of Valencia, Spain has managed the setup and launch of experimental sites in Spain for the calibration of thermal infrared sensors and the validation of LST products derived from those data (Sobrino and Skokovic, 2016). Currently, three sites have been identified and equipped (Fig. 6): the agricultural area of Barrax (39.05 N, 2.1 W), the marshland area in the National Park of Doñana (36.99 N, 6.44 W), and the semi-arid area of the National Park of Cabo de Gata (36.83 N, 2.25 W). These stations have been involved in the validation of LST products derived from a number of Earth Observation sensors: SEVIRI, MODIS, and TIRS/Landsat-8.

Figure 6. Test sites locations (up) and plots (down) of the fixed stations. From left to right: Doñana (Cortes, Fuente Duque and Juncabalejo), Cabo de Gata (Balsa Blanca) and Barrax (El Cruce and Las Tiesas) test sites. From Sobrino and Skokovic (2016).

Thermal radiances measurements are collected over the test sites using IR120 (Campbell Scientific) and Apogee broadband radiometers (8-14 μm). Calibration of the radiometers is performed every 6 months in the laboratory, ensuring the accuracy of the measurements. Because minimal differences of ±0.2 K between two consecutive calibrations were observed, a period of 6 months was considered adequate for calibration frequency. The measurements of the radiometers are performed every 10 seconds, storing the 5-minute average data. In order to obtain the LST from the measurements, surface leaving radiances are corrected for emissivity and reflected down-welling irradiance. At each station emissivity values are obtained on a bimonthly basis in order to account for annual changes. With the CIMEL CE 312-2 multiband radiometer, spectral emissivities are obtained by applying the Temperature and Emissivity Separation (TES) method to the thermal radiances (Jiménez-Muñoz and Sobrino, 2007). Because the CIMEL and the broadband radiometers present slight spectral differences, a comparison between broadband emissivities and the ASTER spectral library is performed to adjust the estimated emissivity and assess the uncertainty range. In addition to emissivity, down-welling radiance is estimated from MODTRAN-5 radiative transfer calculations for the MODIS MOD07 atmospheric profiles and the radiometer's spectral response function.

Regarding the spatial representativeness of the measurements, Juncabalejo, Fuente Duque (in Doñana) and Balsa Blanca (in Cabo de Gata) have adequate homogeneity for moderate (~1km) and high (<100m) resolution sensors (average dispersion below 1 K) while El Cruce, Las Tiesas (in Barrax) and Cortes (in Doñana) are suitable for moderate resolution sensors, with average dispersion of 0.5 K.

3.3.1.6 KIT stations

Karlsruhe Institute of Technology (KIT) stations were designed to allow the continuous validation of LST products over several years (Table 6). In order to minimize complications from spatial scale mismatch

between ground-based and satellite sensors, the stations were set up in large, flat areas with homogenous surface cover. Furthermore, the stations are located in different climate zones, which allow analyses of LST products under different atmospheric conditions and over broad temperature ranges (Fig. 7).

Table 6. List of KIT validation stations including geolocation, elevation, surface emissivity (MSG/SEVIRI channel 10.8 µm) and basic description of the surface type at station location and around the station within moderate resolution satellite footprints.

Site location	**Latitude**	**Longitude**	**Elevation**	**Surface type at station**	**Surface type around station**	**Surface emissivity**
Evora, Portugal	38.540° N	8.003° W	230 m	Savanna, woody savanna	Savanna, woody savanna	0.978
Dahra, Senegal	15.402° N	15.433° W	90 m	Bare ground, grassland	Bare ground, grassland	0.950 - 0.980
Gobabeb wind tower, Namibia	23.551° S	15.051° E	406 m	Bare ground, dry grass	Bare ground, dry grass	0.944
Farm Heimat, Kalahari, Namibia	22.933° S	17.992° E	1380 m	Shrubland	Shrubland	0.973 - 0.984

The core instruments of KIT's validation stations are Heitronics KT15.85 IIP (KT15) infrared radiometers that measure radiances between 9.6 and 11.5 µm. The temperature resolution of the KT15.85 IIP is given as 0.03 K with an uncertainty of ±0.3 K over the relevant range, and high stability with a drift of less than 0.01 % per month (Goettsche *et al.*, 2013). This is achieved by linking the radiance measurements to internal reference temperature measurements. Relevant endmembers are observed under a view angle of 30°; using this view angle instead of the nadir view is justified by the fact that the angular emissivity variation of sand, grass, and gravel is negligible up to view angles of at least 30° (Sobrino and Cuenca, 1999). From 25 m height, the KT15's field of view of 8.5° results in a footprint of about 14 m^2. An additional KT15 faces the sky at 53° with respect to zenith and measures the channel-specific downwelling longwave radiance ($L^{\downarrow}_{sky,\lambda}$ in Eq. 6), which is used to correct for the reflected component in the down-looking measurements. All measurements are provided at a sampling interval of 1 min.

The KT15.85 IIP radiometers are checked annually in parallel runs with freshly calibrated reference instruments. All radiometers are initially calibrated to specifications by the manufacturer (Heitronics GmbH, Wiesbaden, Germany). Re-calibration against a blackbody is performed by KIT about every two years and after deployment, e.g. after an exchange of radiometers for new instruments. At Gobabeb, Namibia – a very homogeneous site in terms of land cover, the uncertainty of situ LST measurement is estimated at ±0.8 K and mainly due an emissivity uncertainty of ±0.015 (Goettsche *et al.*, 2016).

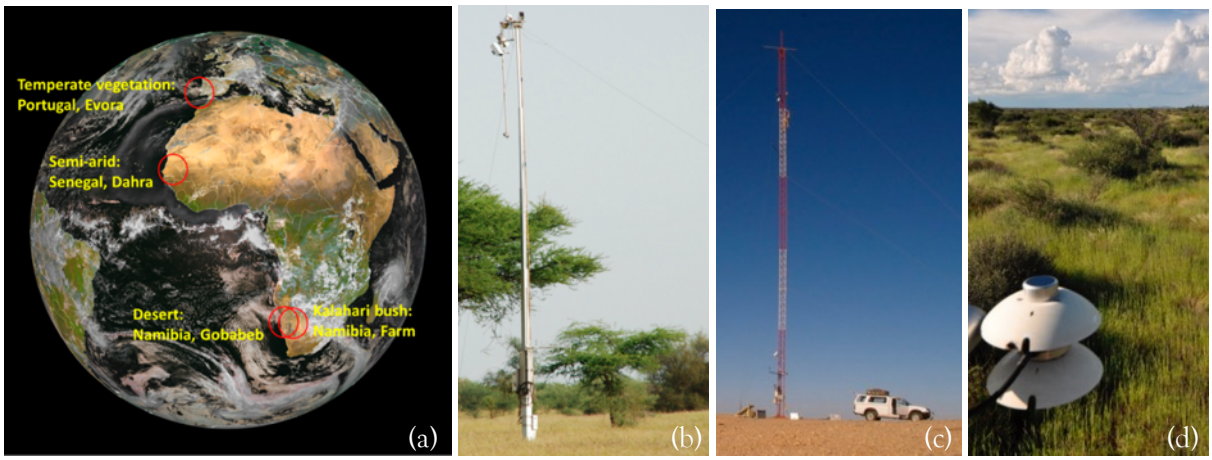

Figure 7. (a) Locations of the KIT's validation stations. African stations at (b) Dahra, Senegal, (c) Gobabeb, Namibia and (d) Farm Heimat, Namibia (Kalahari rainy season).

The IR radiance measurements from KIT stations have been successfully used to validate several satellite LST products derived from MODIS (Freitas *et al.*, 2010; Guillevic *et al.*, 2013; Ermida *et al.*, 2014) and SEVIRI (Freitas *et al.*, 2010; Goettsche *et al.*, 2013; Ermida *et al.*, 2014). The monitoring capability of KIT's validation stations was demonstrated by Göttsche *et al.* (2016) for LST derived from MSG/SEVIRI. For daytime and nighttime data (outside of the rainy seasons), the authors found that the LSA SAF operational LST product generally achieves a RMSE of about 1.5 K, which is better than its target accuracy of 2 K. For daytime MODIS LST obtained over Evora station, which is located in a sparse oak tree savannah, Guillevic *et al.* (2013) quantified the strong directional effects due to canopy structure resulting in a bias of about 4.5 K compared to in situ LST; however, accounting for MODIS viewing configurations with a radiative transfer model reduced it to 0.6 K. Xu *et al.* (2014) used SEVIRI data as proxy to develop the Geostationary Operational Environmental Satellite (GOES)-R Advanced Baseline Imager (ABI) LST algorithm and validated the derived LST with in situ LST from KIT's stations and identified algorithmic weaknesses over arid areas due to a lack of in situ emissivity datasets.

3.3.2 Uncertainties Related to Input Data

The primary uncertainties of ground-based LST retrievals depend on the accuracy of the radiometric measurements and the emissivity estimates used in Eq. 6 and Eq. 7 (Hook *et al.*, 2007; Guillevic *et al.*, 2014; Sobrino and Skokovic, 2016; Göttsche *et al.*, 2016). Depending on the characteristics of the field sensors, the spectral domain to consider can be relatively large, e.g. 9.6-11.5 µm for the Heitronics radiometer, 8-14 µm for the Apogee sensor and 3.5-50.0 µm for standard pyrgeometers. The uncertainty associated with ground-based LST products should be assessed by propagating estimated errors in ancillary information. An example of error budget for the GCU sites (Sobrino and Skokovic, 2016) is provided in Table 7.

Table 7. Example of uncertainty ranges of parameters for in ground-based LST uncertainty estimates (from Sobrino and Skokovic, 2016). Values may depend on specific experimental design.

Quantity	**Uncertainty**	**Estimated impact on in situ LST**
Radiometric calibration	± 0.2 to 0.5 K	0.2 K
Emissivity	± 1%	0.3 K
down-welling atmospheric radiance	± 10%	0.1 K

3.3.2.1 Radiometric calibration

Field radiometers should be calibrated (e.g. to better than ±0.3 K) and traceable to primary reference blackbodies, e.g. from the National Physical Laboratory (NPL), Physikalisch-Technische Bundesanstalt (PTB), or the National Institute of Standards and Technology (NIST). For long-term observations, field radiometers should be controlled and eventually calibrated on a regular basis (once or twice per year ideally, depending on instrument type). Calibration should be performed in a laboratory. Portable blackbody systems exist and may allow in situ radiometer calibration; however, such measurements are not trivial and are difficult to do in the field due to environmental conditions, such as atmospheric radiation and radiation from the target environment for instance (Göttsche *et al.*, 2017).

When multiple sensors are deployed at a site (aiming at the target, multiple surface end-members or the sky for example), a radiometric adjustment or cross calibration is needed. Although limited by their natural heterogeneity and spatial LST variability, surfaces that are approximately homogeneous on the spatial scale of the ground-based radiometer can be used for inter-calibration. The following practical field methods for inter-calibrating radiometers can be used (Theocharous *et al.*, 2016):

- Inter-calibration of same-type radiometers: radiometers are aligned to a common target, which should be as homogeneous and isothermal as possible. Deviations between individual brightness temperature (BT) measurements (from mean BT) exceeding a certain threshold, i.e. twice the radiometer's precision (standard deviation), indicate instrumental problems and require re-calibration. Suitable conditions and natural targets are water, sand, dense grass/crop under clear sky.
- Identical 'sky' radiometers can be inter-calibrated using a sequence of zenith angles, e.g. from 70° (and thus avoiding the horizon) to 0°, which typically provides a range of brightness temperature values (BT) from below surface air temperature to zenith sky BT.
- Inter-calibration of different radiometer types (e.g. different spectral response functions, directional versus hemispherical measurements) requires targets with spectrally constant emissivity and negligible surface anisotropy such as water bodies or dense grass/crop.

Results of calibration, inter-calibration and re-calibration performed before, during or after a field campaign should be meticulously analyzed and reported in the validation summary. The following field (inter-)calibration protocol for TIR radiometers is proposed (Theocharous *et al.*, 2016):

- Ideally, radiometers are re-calibrated against a blackbody (e.g. at the high and low end of the expected temperature range) before and after a field campaign.
- All observations should be performed at the same near-nadir view angle (<30°) and at the same azimuth angle to minimize differences due to directional viewing effects.
- Radiometers with different field of view should be inter-calibrated over surfaces with negligible anisotropy, e.g. dense rice fields.
- Radiometers with different spectral ranges should be inter-calibrated over surfaces with constant emissivity (e.g. water).
- Radiometer intercalibration over natural surfaces requires that sensor footprints represent similar homogeneous and isothermal surface areas. Spatial LST variability over homogeneous surfaces is

usually low for low wind speed conditions and under completely clear or cloud-covered skies; at nighttime land surfaces are often close to isothermal and provide the most favorable inter-calibration conditions.

3.3.2.2 Surface emissivity

Reliable information about the surface emissivity of the validation site (e.g. accurate measurement or best estimate and associated uncertainties) must be available in order to convert measurements of brightness temperature into in situ LST and estimate the impact of emissivity uncertainty on the retrievals (Göttsche *et al.*, 2016). Only few validation teams are conducting in situ emissivity measurements/estimates. At the Gobabeb site in Namibia, Goettsche and Hulley (2013) used the 'one-lid emissivity box' method (Rubio *et al.*, 2003) to estimate the surface emissivity. The one-lid method is well suited over open, relatively flat, and unobstructed field sites with frequent clear sky conditions. In contrast, the 'two-lid emissivity box' method is more complex and provides lower signal-to-noise, but nearly independent of environmental conditions (Sobrino and Caselles, 1993).

A second approach for emissivity validation involves gathering samples of materials in the field and then measuring their emissivity in a controlled laboratory environment. This method assumes the samples collected are representative of the sensor's field of view and has been used extensively for the validation of Advanced Spaceborne Thermal Emission and Reflection Radiometer (ASTER) emissivity retrievals (Hulley *et al.*, 2009; Sabol *et al.*, 2009; Schmugge and Ogawa, 2006). The emissivity of the field samples is determined using a Nicolet 520 FT-IR spectrometer equipped with a Labsphere integrating sphere (Baldridge *et al.* 2009). Each spectrum is then convolved with the appropriate satellite response function. The uncertainty associated with the Nicolet FT-IR emissivities is 0.002 (0.2 %) (Korb *et al.*, 1999).

Another approach is to apply the Temperature Emissivity Separation (TES) algorithm originally developed by Gillespie *et al.* (1998) to obtain satellite emissivity from ASTER data, e.g. Jiménez-Muñoz and Sobrino (2007) used TES to derive spectral emissivity estimates from thermal radiances measured by a multiband field radiometer. For wide band-instruments, the broadband surface emissivity used in Equation 7 can be estimated from a spectral-to-broadband relation (Ogawa *et al.*, 2008) using the ASTER Global Emissivity Dataset (GED v3; Hulley and Hook, 2009b) following Guillevic *et al.* (2012, 2014). The emissivity integrated between 8 and 13.5 μm is commonly assumed to be the best estimate of the broadband emissivity (Ogawa *et al.*, 2008; Cheng *et al.*, 2013). Whereas for spatially and temporally homogeneous validation sites, such as Lake Tahoe, it is sufficient to provide a single value for emissivity, heterogeneous sites require an estimation of multiple emissivity values for each of the site's endmembers (Ermida *et al.*, 2014). In addition, the emissivity of certain scene endmembers changes throughout the year in response to the phenology of the vegetation. In such cases, it is necessary to obtain representative seasonal emissivity estimates - at least representing the major changes in emissivity. If in situ emissivity measurements are not available then emissivity values from the ASTER spectral library (Baldridge *et al.*, 2009) could instead be used for each endmember.

3.3.2.3 Atmospheric downwelling radiance

The atmospheric downwelling radiance represents the hemispherical incoming radiation emitted by the

atmosphere. Except for a few sites such as those within Fluxnet, SURFRAD, or KIT neither spectral nor directional measurements of downwelling thermal radiation from the atmosphere is routinely sampled in the field. The pyrgeometers installed on the Fluxnet or SURFRAD towers directly provide a hemisphere-integrated radiance whereas KIT stations have dedicated radiometers which measure sky brightness temperature at the so-called 'representative zenith angle' of about 53° (Kondratyev, 1969; Unsworth, 1975; Goettsche, 2013). Whether derived from models (e.g. Brutsaert, 1975; Idso, 1981; MODTRAN; RTTOV) or in-situ radiance measurements, estimates of hemisphere-integrated downwelling radiance can have significant uncertainties, especially for warm and humid atmospheres. Ideally, radiosondes measuring the atmospheric profiles of air temperature and water vapor will be launched concurrently to the satellite overpass at or in close proximity to the validation site (Wan and Li, 2008; Schneider *et al.*, 2012). Atmospheric profiles of air temperature and water vapor content can also be retrieved from reanalysis datasets provided, for example, by the European Center for Medium range Weather Forecasting (ECMWF; Uppala *et al.*, 2005; Dee *et al.*, 2011), NCEP (Kalnay *et al.*, 1996) or the Global Modeling and Assimilation Office (GMAO) (Rienecker et al, 2011). Garcia-Santos *et al.* (2013) compared hemispherical downwelling irradiance obtained from in-situ measurements with that obtained from radiative transfer calculations for atmospheric profile data: for clear-sky conditions and an unobstructed upper hemisphere the methods produced comparable results. However, when based on reanalysis datasets, the performance of the validation effort can be significantly reduced due to spatial and temporal matching issues between the reanalysis data and the satellite footprint and overpass time, respectively.

3.3.3 Geometric Considerations

LST products are based on satellite measurements whose effective projected instantaneous field of view (EPIFOV), in general, will not exactly match the mapping unit due to two main reasons:

- The change in pixel size due to across track scan-angles further from nadir, i.e. the pixel size on the ground increases with distance from the sub-satellite point (up to five times the value at nadir for wide swath whisk broom systems).
- Terrain effects change the shape, nominal location and to a lesser extent size of the ground projected instantaneous field of view (PIFOV). Certain processing chains (such as the MODIS adaptive processing system [MODAPS]) apply orthorectification to provide a precise nominal location for all terrain. However, the majority of sensor processing chains do not include orthorectification by default. It should be noted that no current processing chain accounts for the variable shape of the PIFOV.

Depending on canopy structure, sun illumination and viewing direction, satellites measure different surface radiometric temperatures, particularly over sparsely vegetated regions and open canopies, e.g. due to shadowing effects (Guillevic *et al.*, 2013). The impact of directional effects on satellite LST products has been described by Guillevic *et al.* (2003, 2013), Rasmussen *et al.* (2011), Lagouarde *et al.* (2000), Pinheiro *et al.* (2006), Sobrino *et al.* (2005) and Trigo *et al.* (2008), for example. Previous multi-sensor comparison studies (Trigo *et al.*, 2008; Guillevic *et al.*, 2013; Ermida *et al.*, 2014) found differences up to 12 K between MODIS and SEVIRI-derived LST over sparsely vegetated woodlands due to directional effects related to combinations of view angle, sun position and associated shadowing effects. Pinheiro *et al.* (2006) and Trigo *et al.* (2008) found similar differences in directional field radiometer measurements over woodlands in

Africa and Portugal, respectively.

Appropriate matchups significantly reduce the discrepancies induced by directional effects such as shadows and variable footprint size. However, the impact of differences in spatial resolutions, spatial weighting and spectral responses on validation results remains difficult to assess and cannot be completely eliminated.

3.4 Reference LST Estimates

Reference LST estimates are required to evaluate the accuracy and to a lesser extent the spatial and temporal precision of satellite-based LST products. These estimates can be obtained from in situ measurements or heritage LST datasets. However, assuming that in situ LST are obtained from independent measurements, the direct comparison of satellite-derived LST against in situ LST is the only 'true' validation approach. Accurate in situ observations of LST from a suitable site that is representative of at least several pixels in the satellite field of view, and measured contemporaneously with the satellite overpass, arguably offer the highest-quality validation reference that can currently be achieved (Schneider *et al.*, 2012). Unfortunately, due to the high cost and complexity of operating dedicated and highly reliable in situ LST validation stations, the number of available sites is relatively low on a global scale (<20). The following sections survey approaches that have been used to obtain in situ reference LST estimates and identify good practices related to their production.

3.4.1 The Elementary Sampling Unit (ESU) Mapping Unit

Most good practices for LST validation require an estimate of the spatial mapping unit corresponding to each sampled ESU. The ESU mapping unit should correspond to the area over which the LST together with its associated measurement error are representative. The ESU should also be large enough to be either directly co-located with LST product mapping units or with ancillary information than can be used to upscale one or multiple ESUs over a region. The ESU could also include a means of estimation of measurement precision such as replicate sampling. These considerations often drive the specification of the ESU mapping unit.

Heterogeneous sites require the use of multiple radiometers, at least one for each endmember. For sparse woody area in semi-arid environment, this should also include sampling of shadow areas due to vegetation canopy structure (Ermida *et al.*, 2014). In such cases, a geometric projection model can help to estimate the contribution of each surface endmember in the at-sensor radiometric measurement (e.g. Guillevic *et al.*, 2013; Trigo *et al.*, 2008). According to results obtained for MODIS and VIIRS (Wang *et al.*, 2008; Guillevic *et al.*, 2012, 2014), we strongly recommend to perform ground-based LST validation over highly homogeneous sites only. High-resolution LST or normalized difference vegetation index (NDVI) datasets can be used to evaluate the spatial representativeness of in situ LST measurements and to select appropriate validation sites, but more sophisticated approaches exist, such as empirical variograms used by Román *et al.* (2009), to estimate the spatial variability of surface albedo around stations of interest.

3.4.2 ESU LST Uncertainty

The performance of a validation exercise strongly depends on the uncertainty of the reference LST

datasets. Reference LST uncertainties should be meticulously reported, including uncertainties associated with the upscaling or geometric models used, and to some extent, the uncertainty associated with the representativeness of the ESU.

3.4.3 Upscaling of Reference LST Estimates

LST in situ reference needs to represent the entire satellite footprint. While one well-calibrated radiometer (i.e. single LST ESU) can represent a good reference LST estimate for homogeneous sites, validation efforts over heterogeneous sites in terms of land cover or canopy architecture require robust scaling methods (Guillevic *et al.*, 2014; Göttsche *et al.*, 2016). On a practical basis, ESUs represent areas of around 1ha (100 m · 100 m) or smaller. Depending on the experimental design, the footprint diameter of ground-based TIR instruments typically range from 1 to 10 m for spectral radiometers and from 10 to 100 m for pyrgeometers (Fig. 8). The spatial representativeness of ground-based LST derived from SURFRAD pyrgeometer measurements is around 70 m × 70 m for example. However, most vegetated landscapes contain various land cover types or soils and, therefore, the LST observed by a station at one specific location usually does not represent the surrounding area that is included in the lower resolution satellite sensor footprint (e.g. 1 km^2). Spatial scaling of ESU measurements can reduce uncertainties and increase the spatial representativeness of in situ measurements. Spatial scaling methods are generally based on information describing (directly or indirectly) the LST spatial variability and a model to scale in situ measurements to satellite spatial resolution. LST spatial variability can be characterized with multiple in situ radiometers, high resolution LST imagery or using a predictor variable such as vegetation density or NDVI. For example, the scaling method developed by Guillevic *et al.* (2012, 2014) to validate LST products derived from MODIS and VIIRS was based on the use of a land surface model to quantify differences in subpixel temperature between classes of surface biophysical properties (i.e. different surface types or different vegetation densities) with respect to the LST measured by the station– see appendix for additional information about the method.

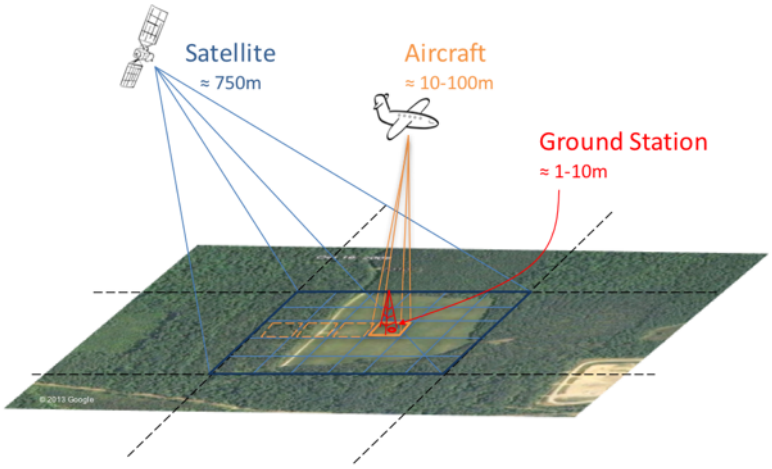

Figure 8. Representation of scaling and directional effects.

3.4.4 Temporal sampling

Ideal in situ measurements of LST need to be continuous in time with a temporal sampling rate

ranging from 1 to 3 minutes. Less frequent observations can still be helpful but generally result in either significantly fewer matchups between satellite and in situ LST or in a higher validation uncertainty. For significant time differences (but < 30 minutes) in situ LST need to be temporally interpolated to satellite overpass time. Temporal differences exceeding 30 minutes between are unsuitable for validation purposes.

4 GENERAL STRATEGY FOR VALIDATION OF LST PRODUCTS

Through the efforts of space agencies, as well as a number of research groups, the global community now has open access to moderate resolution (750m – 1km) global LST datasets from MODIS, VIIRS and SLSTR, and high temporal resolution data (15 minutes – 1 hour) from geostationary satellites (GOES and SEVIRI). However, these datasets have limitations and may include variable levels of quality assessment.

4.1 CEOS Validation Stages

The CEOS WGCV Land Product Validation (LPV) subgroup has identified four validation levels corresponding to increasing spatial and temporal representativeness of samples used to perform direct validation (Table 8). The LST validation protocol includes these aspects and supplements them with requirements for assessing the spatial and temporal precision of individual products.

Table 8. The CEOS WGCV Land Product Validation Stages.

Stage 0 Validation	No validation results have been reported.
Stage 1 Validation	Product accuracy is assessed from a small (typically < 30) set of locations and time periods by comparison with in situ or other suitable reference data.
Stage 2 Validation	Product accuracy is estimated over a significant set of locations and time periods by comparison with reference in situ or other suitable reference data. Spatial and temporal consistency of the product with similar products has been evaluated over globally representative locations and time periods. Results are published in the peer-reviewed literature.
Stage 3 Validation	Uncertainties in the product and its associated structure are well quantified from comparison with reference in situ or other suitable reference data. Uncertainties are characterized in a statistically robust way over multiple locations and time periods representing global conditions. Spatial and temporal consistency of the product and consistency with similar products has been evaluated over globally representative locations and periods. Results are published in the peer-reviewed literature.
Stage 4 Validation	Validation results for stage 3 are systematically updated when new product versions are released and as the time-series expands.

4.2 Status of Current Validation Capacity and methods

The objective of validation efforts is to characterize product uncertainties and evaluate the performance of retrieval algorithms. Identified issues with a retrieval algorithm and/or ancillary datasets used by the algorithm should be immediately reported to the algorithm development team for algorithm refinement.

4.2.1 Methods

Multiple validation methods and activities are necessary to assess LST compliance with specifications. A

detailed presentation of previous satellite-based LST validation efforts is available in the review by Li *et al.* (2013). Four different methods have been widely used to validate and determine the uncertainties in LST products derived from satellite measurements (Schneider *et al.*, 2012; Guillevic *et al.* 2014): ground-based validation, satellite products inter-comparison, radiance-based validation and time series inter-comparison methods.

4.2.1.1 Ground-based validation

This approach involves comparisons with ground-based measurements of LST, and has been frequently used to validate LST products retrieved from MODIS (Bosilovich, 2006; Coll *et al.*, 2005, 2010; Guillevic *et al.*, 2012, 2013; Hook *et al.*, 2007; Trigo *et al.*, 2008; Wan, 2008; Wang *et al.*, 2008; Wang and Liang, 2009), SEVIRI (Göttsche *et al.*, 2013, 2016; Martin and Göttsche, 2016; Guillevic *et al.*, 2013; Kabsch *et al.*, 2008; Trigo *et al.*, 2008), the Advanced Very High Resoluion Radiometer (AVHRR) (Prata, 1994), ASTER (Sobrino *et al.*, 2007), ATSR (Prata, 1994), VIIRS (Guillevic *et al.*, 2014; Li *et al.*, 2014) and AATSR (Ouyang *et al.*, 2017; Martin and Göttsche, 2016). The two main limitations of this approach are the spatial representativeness of the in situ reference measurements and directional effects (Guillevic *et al.*, 2013, 2014; Ermida *et al.*, 2014; Göttsche *et al.*, 2016). For most mixed vegetated landscapes composed of various land cover types or soils, the LST measured by a station does not represent the surrounding area that is part of the coarser satellite sensor footprint (Guillevic *et al.*, 2012, 2014; Göttsche *et al.*, 2016). Moreover, most field radiometers collect observations near nadir, whereas wide field-of-view satellite scanners like MODIS and VIIRS collect observations from nadir to around 60° view angle. The method is particularly suited for studies over inland water bodies which provide large spatially homogenous targets and can be used to both evaluate and improve the performance of retrieval algorithms (Coll *et al.*, 2009a; Guillevic *et al.*, 2014; Hook *et al.*, 2007; Hulley *et al.*, 2011). Therefore, in situ reference data are selected based on the following criteria: networks with high quality instrumentation and maintenance, and good spatial representativeness for the satellite sensor footprint. **Comparisons with ground-based measurements represent the reference validation method** and there are critical needs for the development of denser ground-based reference networks: two different satellite LST products can be in very good agreement since they use a similar algorithm, however they may differ considerably from the corresponding ground-based reference measurements (Fig. 9, Guillevic *et al.*, 2014).

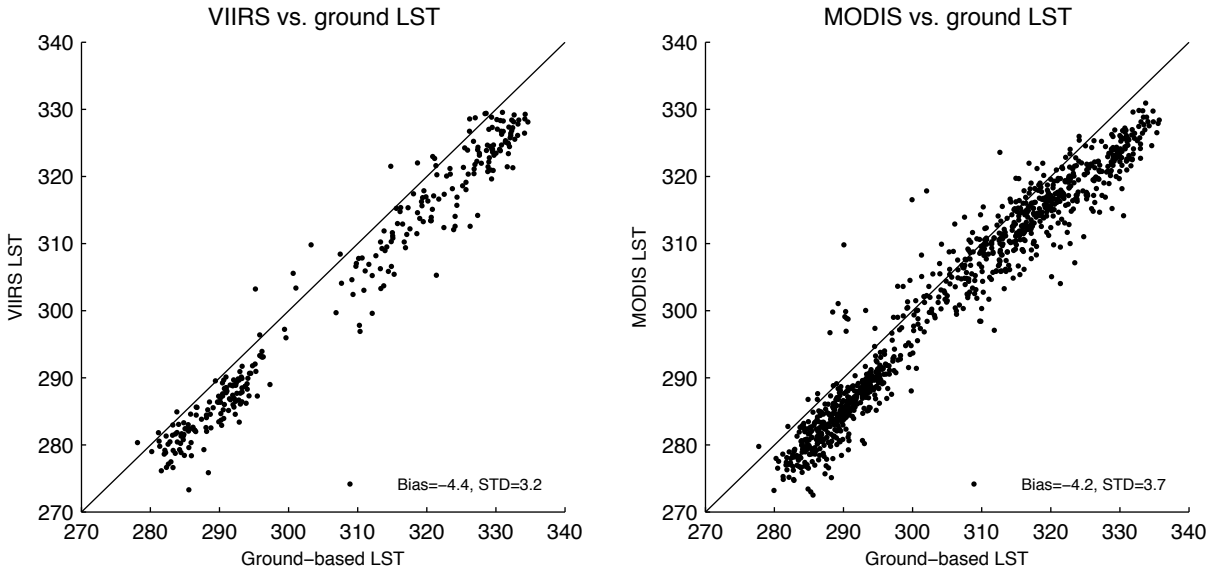

Figure 9. VIIRS (left) and MODIS (right) LST products versus ground-based LST measurements at the KIT stations in Gobabeb, Namibia. Due to an overestimation of surface emissivity values used in the algorithms, both VIIRS and MODIS products significantly underestimate the LST of the Namibian desert by more than 4 K on average (From Guillevic *et al.*, 2014). The figure illustrates the critical needs for ground-based reference: two different satellite LST products can be in very good agreement since they use a similar algorithm, however they may differ considerably from the corresponding ground-based reference measurements.

4.2.1.2 Satellite product Inter-Comparison

This approach involves comparing a new satellite LST product with a heritage LST product (Martin *et al.*, 2016; Guillevic *et al.*, 2013, 2014; Hulley and Hook, 2009; Jacob *et al.*, 2004; Trigo *et al.*, 2008). The method is particularly valuable for finding spatial disagreements between LST products over large areas and for a wide range in cover types. However, the approach does not yield absolute validation results and satellite LST inter-comparisons alone are insufficient to validate a new product, i.e. different retrieval algorithms based on similar assumptions and formulations (e.g. split-window) can be highly consistent with each other but biased when compared to ground reference LST (Guillevic *et al.*, 2014). The inter-comparison approach requires accounting for differences in spatial resolution, view angle and overpass time between the satellite datasets. Different observations are never strictly simultaneous and the differences in sensor footprint increase with differences in viewing geometry. In order to reduce the effect of cloud contamination on validation results, only cloud free data should be used. Furthermore, different periods of the year associated with dry and wet atmospheres should be considered to detect possible seasonal effects on the observed LST differences. The spectral response of each instrument is accounted for by the retrieval algorithms. The impact of directional effects on satellite LST products has been described by Guillevic *et al.* (2003, 2013), Rasmussen *et al.* (2011), Pinheiro *et al.* (2006), Sobrino *et al.* (2005) and Ermida *et al.* (2017a). Matchups represent coincident pairs of granules with respect to satellite overpass times and view angles. These "near miss" time spans are usually referred to as Simultaneous Nadir Overpasses (SNOs) when nadir view angles are considered (Cao *et al.*, 2004). For LST product intercomparisons, we recommend to select data with view angles lower than 45°, a satellite angular separation limit of ±10° and a satellite time separation limit of ±10 minutes. In their study, Guillevic *et al.* (2014) found large differences (up to 15 K)

between MODIS and VIIRS LST products over arid and semi-arid regions under temperatures exceeding 320 K and high atmospheric water vapor content conditions (Fig. 10).

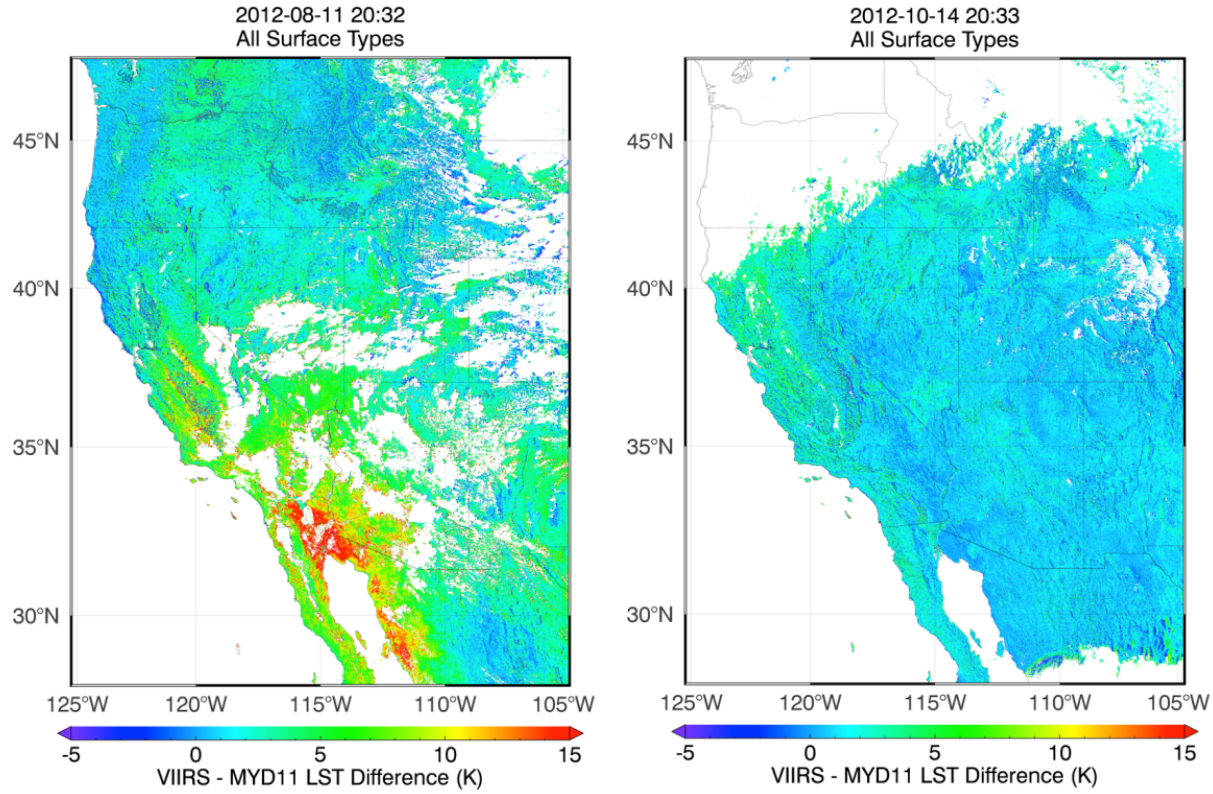

Figure 10. Differences between VIIRS and MODIS (MYD11) LST products observed over the western USA on two different dates associated with different atmospheric conditions: hot and wet in August 11, 2012, cool and dry in October 14, 2012. The white areas over land are regions where good-quality retrievals were not available (e.g., clouds) (From Guillevic *et al.*, 2014).

These differences were caused by an insufficient sampling of environmental conditions, i.e. atmospheric conditions and surface temperatures, when determining the VIIRS algorithm coefficients. For very humid atmospheres, large differences between the VIIRS brightness temperatures strongly enhanced the contribution of the quadratic term in the algorithm formulation (Eq. 4).

4.2.1.3 Radiance-based Validation

The Radiance-based (R-based) method does not require in situ measurements, but instead requires accurate estimates of channel specific surface emissivity values, as well as atmospheric temperature and water vapor profiles coincident with the satellite overpass (Coll *et al.*, 2009b; Hulley and Hook, 2012; Niclòs *et al.*, 2011; Wan and Li, 2008; Wan, 2014). The advantage of the R-based method is that it can be applied to a large number of global sites where the emissivity is known (e.g., from field measurements) and during night- and daytime observations to define the diurnal temperature range. The R-based method is based on a 'radiative closure simulation' with input surface emissivity spectra from either lab or field measurements, atmospheric profiles from an external source (e.g., model or radiosonde), and the retrieved LST product as

input. A radiative transfer model is used to forward model these parameters to simulate at-sensor BTs in a clear window region of the atmosphere (11–12 μm). The input LST value is then adjusted in 2-Kelvin steps until two calculated at-sensor BTs bracket the observed BT value. An estimate of the 'true' temperature is then found by interpolation between the two calculated BTs, the observed BT, and the initial retrieved LST used in the simulation. The LST error, or uncertainty in the LST retrieval is simply found by taking the difference between the retrieved LST product and the R-based LST. This method has been successfully applied to MODIS LST products in previous studies (Coll *et al.* 2009; Wan and Li 2008; Wan 2008) as well as AIRS LST validation (Hulley and Hook 2012). For MODIS data, band 31 (10.78–11.28 μm) is typically used for the simulation since it is the least sensitive to atmospheric absorption in the longwave region.

Wan and Li (2008) proposed a quality check to assess the suitability of the atmospheric profiles by looking at differences between observed and calculated BTs in two nearby window regions with different absorption features. For example, the quality check for MODIS bands 31 and 32 at 11 and 12 μm is given by Equation 9:

$$\delta(T_{11} - T_{12}) = \left(T_{11}^{obs} - T_{12}^{obs}\right) - \left(T_{11}^{calc} - T_{12}^{calc}\right) \tag{9}$$

where: T_{11}^{obs} and T_{12}^{obs} are the observed brightness temperatures at 11 and 12 μm respectively, and T_{11}^{calc} and T_{12}^{calc} are the calculated brightness temperatures from the R-based simulation at 11 and 12 μm respectively. If $\delta(T_{11} - T_{12})$ is close to zero, then the assumption is that the atmospheric temperature and water vapor profiles are accurately representing the true atmospheric conditions at the time of the observation, granted the emissivity is already well known. Because water vapor absorption is higher in the 12-μm region, negative residual values of $\delta(T_{11} - T_{12})$ imply the R-based profiles are overestimating the atmospheric effect, while positives values imply an underestimation of atmospheric effects. A simple threshold can be applied to filter out any unsuitable candidate profiles for validation. Although Wan and Li (2008) proposed a threshold of ±0.3 K for MODIS data, Hulley and Hook (2012) performed a sensitivity analysis and found that a threshold of ±0.5 K resulted in a good balance between the numbers of profiles accepted and accuracy of the final R-based LST. An example of Radiance-based LST validation result is presented in Figure 11.

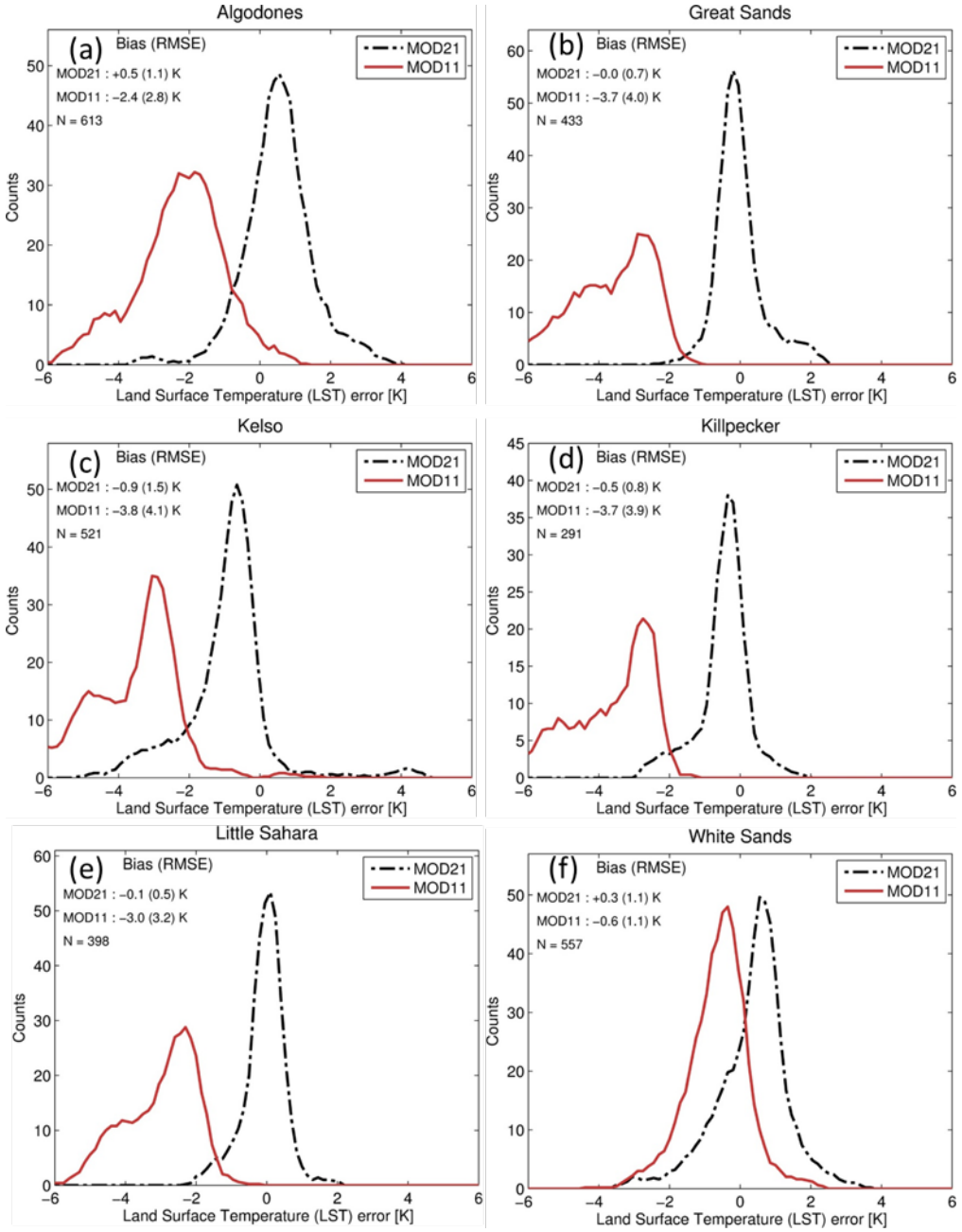

Figure 11. An example of the R-based validation method applied to the MODIS Aqua MOD11 and MOD21 LST products over six pseudo-invariant sand dune sites using all data during 2003-2005. Since very few in situ measurements of LST exist over arid regions, the R-based method is the only objective means to validate satellite LST products over these types of land surfaces over long time periods. In this case the R-based method exposed a 3-5 K cold bias in the MYD11 LST product due to overestimation of desert emissivity values.

4.2.1.4 Time series Inter-Comparisons

This method is used to detect problems that can occur during an instrument's life, e.g. calibration drift (Hook *et al.*, 2007), or unrealistic outliers due to undetected clouds (Merchant *et al.*, 2013). However, the approach requires relatively long time series of observations over temporally highly stable targets, e.g. inland water bodies (Hook *et al.*, 2007). The NASA JPL's instrumented buoys have been used to monitor level-1

radiances or LST products of multiple satellite instruments, such as ASTER (Hook *et al.*, 2007), MODIS (Hook *et al.* 2010), Multispectral Thermal Imager (MTI) (Hook *et al.*, 2005), Landsat (Hook *et al.*, 2004; Barsi, Hook, *et al.*, 2007), and VIIRS (Guillevic *et al.*, 2014). Recently, these measurements have been used to quantify the radiometric problem observed on Landsat 8 (Barsi *et al.*, 2014).

The four different validation approaches are complementary and provide different levels of information about the quality of the retrieved LST. Due to the lack of global reference datasets, these four methods are required to achieve Stage-3 validation status (LPV validation stage are defined in table 7). In general, ground-based LST and state-of-the-art satellite-derived LST products are expected to agree to within 1-2K over homogeneous sites for most conditions. Direct ground-based validation is currently considered as the reference validation method and should be used whenever possible. However, due to the relatively small number of high quality LST validation stations, several validation methods and activities are necessary to assess a LST product's compliance with its specifications.

4.3 Validation Strategy

A general validation strategy should be capable of testing products for compliance with GCOS requirements. A distinction is made between the strategy, which corresponds to the sampling design, the definition of key reference datasets and inter-comparison methods, and the data required to use this strategy to test if products meet either threshold or science requirements. The validation strategy has major criteria detailed in the following sub-sections:

- Direct validation on a global basis representative of surface types and seasonal conditions;
- Quantify the representative LST accuracy estimate over areas or time periods without reference datasets
- Quantify the long term (inter-annual) stability in LST products

4.3.1 Direct validation on a global basis representative of surface types and seasonal

Direct validation (ground-based and radiance-based methods) relies on reference datasets traceable to in situ reference measurements accompanied by an associated assessment of their uncertainty. Reference in-situ LST should take into account the spatial variability and representativeness of the in situ measurements and scaling if necessary. Up-scaling methods should be based on higher resolution information of the surface spatial variability using not only LST but auxiliary variables such as vegetation density and/or albedo derived from high-resolution satellite imagery. Matchups of spatially and temporally coincident product and reference values should be compared using appropriate robust statistics and visualization of residuals. **It is recommended to provide validation results for each season separately** (e.g. to resolve leaf-on/leaf-off periods of deciduous forests). Results should be stratified by class for the ancillary data, e.g. according to land cover type or total atmospheric water vapor content.

4.3.2 Quantify the representative LST accuracy estimate over areas or time periods without reference datasets

Ideally, uncertainties should be rigorously estimated for a variety of different conditions on a pixel-by-pixel basis before they can be merged and incorporated into a time series of measurements of sufficient length, consistency, and continuity to adequately meet science requirements. An evaluation of LST products

can be done at the global scales using scene-based intercomparisons, but as mentioned in section 4.2.1.2, this method does not represent a complete and independent validation. Current LST datasets are available with quality control information, but do not include a full set of uncertainties. To fill this gap, Hulley *et al.* (2012) have developed the capability to estimate uncertainties in LST and emissivity products for a variety of different retrieval algorithms using a Temperature Emissivity Uncertainty Simulator (TEUSim). The simulator uses radiative transfer simulations, global radiosonde and surface emissivity spectra to quantify and separate error contributions from the potential error sources: 1) algorithm/model error, 2) radiometric noise, or measurement error, 3) atmospheric corrections, 4) undetected clouds, and 5) calibration error. The uncertainties generated from TEUSim are parameterized according to view angle, total column water vapor column, and surface type dependence using a least squares method fit to a quadratic function as follows Equation (*10*.

$$\delta LST = a_o + a_1 TCW + a_2 \mathrm{SVA} + a_3 TCW \cdot SVA + a_4 TCW^2 + a_5 SVA^2 \qquad (10)$$

Where δLST is the LST uncertainty (difference between the simulated and retrieved LST in K), a_i are the regression coefficients that depend on the surface type being observed (vegetation, barren, or mixed pixel), TCW is the total column water vapor (cm), and SVA is the satellite viewing angle. The NDVI values of the pixel can be used to set thresholds to discriminate between the three surface coefficient types. Using this parameterization, LST uncertainties can be estimated on a pixel-by-pixel basis. Figure 9 shows LST uncertainty distributions derived from TEUsim plotted versus TCW and simulated LST for vegetated and barren surfaces. Results illustrate classical issues with the split-window retrieval algorithm due to poor representation of barren surface emissivity values in the algorithm.

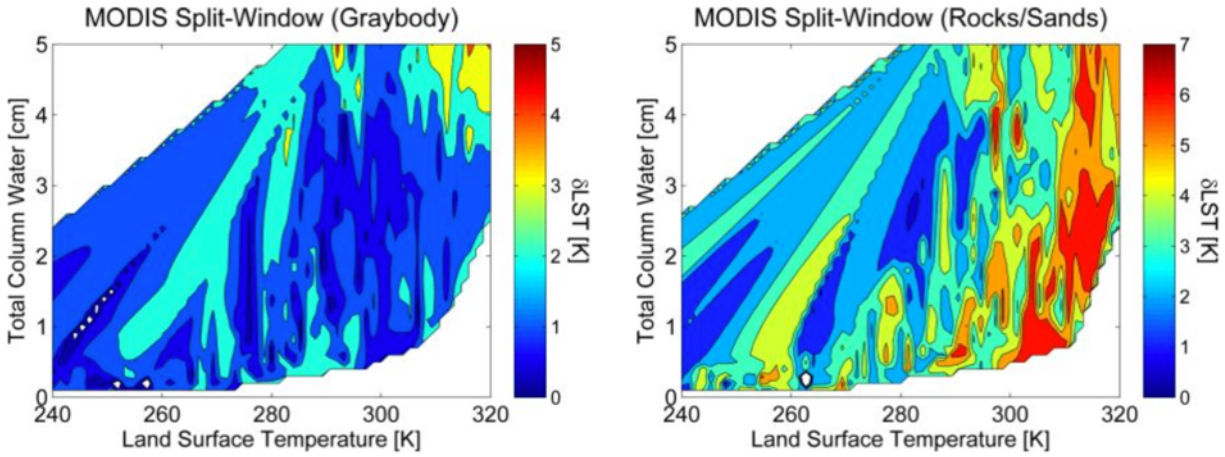

Figure 12. MODIS LST uncertainty distribution derived from TEUsim plotted versus Total Column Water (TCW) and simulated LST for graybody surfaces (left) and barren surface (right).

4.3.3 Quantify the long term (inter-annual) stability in LST products

Calibration of spaceborne instruments has three important aspects: prelaunch determination of instrument calibration, validation of on-orbit performance using on-board measurements, and in-flight vicarious calibration using ground truth. After launch, sensors are susceptible to significant temporal changes in their performance characteristics. The infrared channels of MODIS or VIIRS, for example, form

a self-calibrating radiometer. By using measurements of cold space and of an on-board blackbody calibration target, the infrared measurements are calibrated by producing radiances in the spectral intervals defined by the system response functions of each channel. In-flight vicarious calibration can be performed using time-series inter-comparisons. It requires very stable and homogeneous targets and is usually performed using in situ measurements over water bodies and well-characterized barren surfaces combined with radiative transfer modeling to simulate at-sensor radiances. For water surfaces, data from the JPL's instrumented buoys at Lake Tahoe/Salton Sea (see Section 3.3.1.2) and/or from NOAA moored buoys archived by the National Data Buoy Center (NDBC) have already been used to monitor sensor temporal drift. The NASA JPL buoys were used to monitor level-1 radiances or LST products from multiple satellite instruments, such as MODIS (Hook *et al.* 2007), Landsat (Barsi *et al.*, 2007, 2014) and VIIRS (Guillevic *et al.*, 2014). Schott *et al.* (2012) successfully used NOAA's buoys to verify the calibration of Landsat TM5 and found very consistent results when a large number of buoys were considered. Over land, only a few data sets are appropriate and available for calibration purposes. For example, KIT's validation station in Namibia is used to monitor the performance of the MSG/SEVIRI sensor (Goettsche *et al.*, 2016).

4.4 Reporting Results of LST product Validation

4.4.1 Validation metrics

Definitions for uncertainty, accuracy, precision and completeness applicable to LST validation drawn from experimental statistics are provided in Section 2.4. As a good practice, validation exercises should explicitly define these terms and identify how they relate to the definitions provided in Section 2.4 to facilitate understanding of results across studies. **It is recommended that LST product validation should be performed across a representative sampling of LST magnitudes within a spatial and temporal stratification.** It is good practice to sample across a representative range of LST within a stratification for all performance statistics. It is also good practice to evaluate the precision and completeness of spatial and temporal patterns in addition to reporting statistics based on LST product estimates in a stratum without spatial or temporal considerations. Table 9 summarizes the common practice and recommended good practice.

Table 9. Common practice and recommended good practice.

Quantity	**Current practice**	**Good practice, add:**
Accuracy	Mean difference	Median error Median and percentiles of residuals Box-plots of residuals vs LST
Precision	Standard deviation	Median absolute deviation
Uncertainty	Root mean square error	Scatter plot of match-ups Median and percentiles of absolute residuals, RMSE Box plot of absolute residuals vs LST
Completeness		Gap size distribution

4.4.2 Reporting validation results

Results of validation exercises should be reported publicly after being reviewed by the data producers

and after independent scientific peer review. Reporting in refereed journals is encouraged and supporting materials corresponding to spatial or temporal accuracy statistics should be made accessible. The following details related to reporting results are good practices:

- All participants in the exercise should be declared unless products were provided blindly.
- Links to accessible versions of the products and reference data used during the validation should be provided and maintained.
- Match-ups of product and reference LST values used to derive aggregation statistics together with ancillary information related to location (biome type, latitude and longitude of the site), temporal interval and uncertainty in reference data (at least a reference to the protocol used to produce each reference data point) should be made available publicly.
- Scatter plots and statistics results should be reported within the validation document or linked supplementary material in addition to any other statistics.
- Planned updates or revisions to the document (e.g. in anticipation of new reference datasets that may be available on a regular basis) should be identified.

LST validation studies have used common approaches for reporting algorithm performance although the spatial and temporal extent of the sampling distribution used for comparisons has varied. Statistics are reported to describe the bivariate distribution of reference and product LST, and usually include the Pearson correlation coefficient, bias, standard deviation and root mean square error. However, most validation studies do not test for normal or homeoscedastic distributions of residuals. Such tests should be conducted, especially at the global scale, because it is likely residuals differ for different LST levels that are themselves correlated with biome type or seasonal sampling. Direct comparisons of temporal trends in LST are extremely limited and often assume a small (<1 hectare) site is representative of a larger pixel. This assumption may be appropriate for large fields and homogenous forests but requires care with the in situ protocol and upscaling of reference data to ensure the uncertainty due to this assumption is quantified. Inter-comparisons are commonly conducted at a lowest common resolution to minimize differences due to spatial mismatch. Time-series plots over selected sub-sampled regions, usually by land cover and biome type, should be presented together with maps of inter-product differences on a monthly or seasonal basis.

5 CONCLUSIONS

This document provides CEOS LPV recommendations on good practices for the validation of LST products derived from satellite observations. Validation efforts should include a full characterization and appropriate documentation of the validation datasets used including uncertainty estimates of reference LST measurements (associated with the accuracy of the radiometric measurements, emissivity estimates, ground based retrieval method for example). Because spatial representativeness and directional effects are quite difficult to compensate for, quantitative assessment of algorithm uncertainties requires dedicated and high quality in situ LST measurements over sites that are homogeneous at the spatial scale of the satellite observing system. It is recommended that only sites that are representative of the satellite field of view should be used for validation purposes. Four LST validation approaches have been identified: (1) Ground-based validation, which involves comparisons with LST derived from ground-based radiometric

measurements; (2) Scene-based inter-comparison with heritage LST products; (3) Radiance-based validation, which is based on radiative transfer calculations for known atmospheric profiles and land surface emissivity; (4) Time series comparisons, which are particularly useful for detecting problems that can occur during an instrument's life, e.g. calibration drift or unrealistic outliers due to undetected clouds. LST validation studies should include the four different methods (when applicable) to get a detailed characterization of product accuracies. The four different approaches are complementary and provide different levels of information about the quality of the retrieved LST.

The availability of reference LST data is fundamental for LST validation: currently, LST validation verifies CEOS Level 1 validation stage (see Table 8 for definition) due to the limited number of available reference datasets. The provision of harmonized in-situ and satellite-retrieved LST data sets in a common format, e.g. as promoted and implemented by the ESA DUE GlobTemperature project (www.globtemperature.info), enables researchers to perform (global) LST validation studies more systematically and readily. The LPV subgroup anticipates that spatial representativeness of in situ LST measurements will grow with less expensive in situ survey methods and increasing use of LST products in environmental studies, and that CEOS Level 3 validation can be achieved when the number of sites become more plentiful, distributed and all biomes are represented. However, the limited number of global standard LST products is a fundamental challenge for inter-comparisons since any ensemble of LST products is likely to have biases due to both, the small sample size and the fact that many products are based on very similar algorithm.

6 APPENDIX A: Example of upscaling method using high resolution vegetation data to drive a land surface model

The approach developed by Guillevic *et al.* (2012, 2014) used a physically based land surface model driven by *in situ* atmospheric forcing measurements and high-resolution imagery to describe satellite LST footprints over ground stations. To represent the spatial variability within a satellite pixel, the authors assumed that the sub-pixel temperature variability is mainly due to land cover heterogeneity and variability in surface biophysical parameters, such as vegetation density, emissivity or albedo (Fig. A-1). Because the vegetation transpiration is usually greater than the bare soil evaporation between successive precipitation events, the temperature of vegetated areas under low soil water stress conditions is typically lower than the temperature of barren surfaces. The method estimates the temperature of each land cover class inside a mixed pixel using a land surface model driven by the measured atmospheric forcing and observed surface biophysical properties from a nearby tower/site. The land surface model is used to quantify differences in subpixel temperature between classes of surface biophysical properties (i.e. different surface types or different vegetation densities) with respect to the LST measured by the station. This reduces the impact of model systematic errors and uncertainties in the atmospheric forcing on the assessment of the satellite pixel LST. Guillevic *et al.* (2012, 2014) used a two-source energy balance model that simulates the energy and water transfers between the surface and the atmosphere, and describes the evolution of surface state variables such as LST and soil moisture. In addition to LST estimates, the selected ground stations also provide accurate measurements of local environmental information, in particular the atmospheric forcing required by the model. These measurements include air temperature, relative humidity and wind speed at the surface, and incoming shortwave and longwave radiation. The atmospheric forcing is assumed to be uniform over the satellite footprint, which is approximately 1 km x 1 km for MODIS and VIIRS.

Figure A-1. Spatial variability of land cover type and vegetation density before and after harvest around two NOAA's stations part of the SURFRAD and US CRN network near Bondville, IL.

The different steps of the scaling method are:

– Calibration of the land surface model using ground observations. This task determines the optimal set

of internal model parameters that allows the model to describe the observed *in situ* LST (see Guillevic *et al.* (2012) for a detailed description of the model calibration method).

- Characterization of the satellite footprint, which depends on pixel geolocation, viewing zenith angle, satellite altitude (824 km for S-NPP, and 705 km for Terra and Aqua satellites, for example) and the instantaneous field of view (911 μrad for VIIRS, and 1315 μrad for MODIS at moderate resolution, for example).
- Representation of the LST of each surface end-member using the land surface model forced by the observed biophysical properties at high-resolution. Guillevic *et al.* (2014) used the leaf area index (LAI) derived from MODIS Normalized Difference Vegetation Index (NDVI) standard products at 250m spatial resolution to describe the spatial variability of vegetation density around the station.
- Calculation of LST at satellite resolution from a weighted mean of n radiative contributions from each land cover class (Eq. A.1).

$$LST = \left[\frac{1}{\varepsilon} \sum_{i=1}^{n} f_i \, \varepsilon_i \, T_i^4 \right]^{\frac{1}{4}} \quad with \quad \varepsilon = \sum_{i=1}^{n} f_i \, \varepsilon_i \quad and \quad \sum_{i=1}^{n} f_i = 1 \tag{A.1}$$

where f_i is the cover fraction of land cover class i at temperature T_i and with broadband emissivity ε_i. ε is the broadband surface r-emissivity as defined by Norman and Becker (1995).

The scaling methodology requires high-resolution information about vegetation density. The NDVI is an indicator of green biomass, and an indicator of the photosynthetic efficiency of the plants. Greener areas are usually associated with higher evapotranspiration and, consequently, characterized by lower LST. The validation datasets accounting for scaling is significantly more representative of the satellite footprint (Fig. A.2).

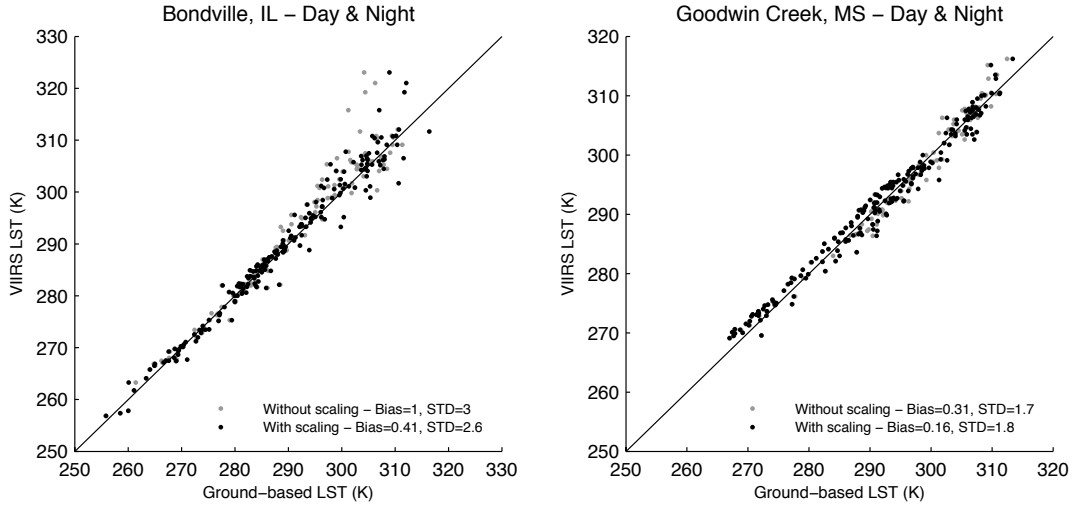

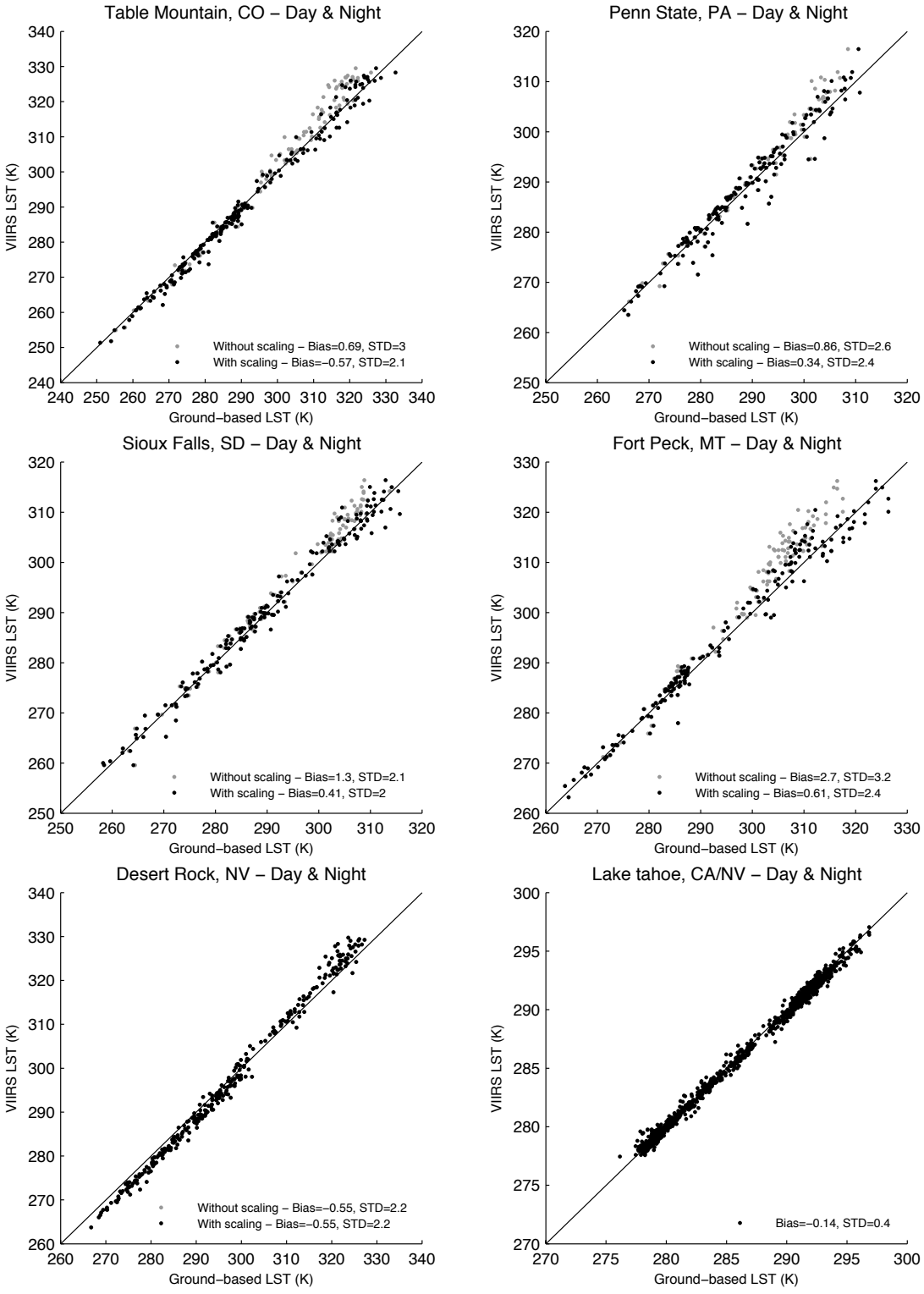

Figure A.2. VIIRS LST product vs. ground-based LST measurements at 8 validation sites (7 SURFRAD stations and JPL buoys at lake Tahoe) representative of various land surface types over the contiguous United States. Results for vegetation sites are with and without scaling (From Guillevic *et al.*, 2014).

7 APPENDIX B: Determination of land surface temperature with thermal infrared in-situ measurements

The reference method for validating satellite-derived LST products is ground-based validation, i.e. comparisons against LST obtained from in-situ measurements with field deployed TIR radiometers (see section 4.2.1.1). In order to qualify for 'category A' validation (Schneider *et al.*, 2012), in situ LST must be derived from completely independent measurements, which need to be fully anchored to SI units and have direct correlation with 'true' surface based quantities. For the convenience of researchers wanting to determine in in-situ LST, this appendix provides the relevant information and best practices from the 'Fiducial Reference Measurements for Validation of Surface Temperature from Satellites (FRM4STS) Technical Report TR-3: A framework to verify the field performance of TIR FRM' (Göttsche *et al.* , 2017). Further information on TIR radiometer calibration and temperature determination over natural surfaces can be found on the ESA FRM4STS project website (www.frm4sts.org).

7.1 LST and emissivity determination with field radiometers

Depending on the particular site, diurnal LST amplitudes of 40 K and surface-overheating of 20 K or more have to be expected. Due to strong surface gradients and local perturbations the thermodynamic temperature at the surface of non-isothermal bodies, e.g. as obtained with thermometers in contact with natural bodies, may be very difficult to measure (Becker and Li, 1995). In contrast, surface-leaving TIR radiance is directly measurable by radiometers, whether they are space borne or ground based. However, the radiance leaving a heterogeneous non-isothermal body depends on its temperature and emissivity distribution, i.e. the fractions with different temperatures in the ground instantaneous field of view (GIFOV) of the radiometer and their respective emissivities. Therefore, an interpretation of the measured radiances over a heterogeneous non-isothermal body in terms of temperature requires additional information about the surface. Before addressing this more general case, we define spectral emissivity and radiometric temperature for a homogeneous isothermal body.

7.1.1 Spectral emissivity

Planck's law relates the radiance emitted by a black body (emissivity $\varepsilon = 1$) to its surface temperature T. However, most objects relevant to remote sensing applications are non-black bodies with $0 < \varepsilon(\lambda) < 1$. Spectral emissivity $\varepsilon(\lambda)$ is defined as the ratio between the spectral radiance R emitted by a surface at wavelength λ and the spectral radiance emitted by a black body $B(T, \lambda)$ at the same wavelength and temperature. Spectral emissivity $\varepsilon(\lambda)$ is then given (Dash *et al.*, 2002):

$$\varepsilon(\lambda) = \frac{R(T,\lambda)}{B(T,\lambda)} \qquad \text{B.1}$$

where ε is assumed to be temperature independent, λ is in meters, R is in W m^{-3} sr^{-1}, and T is in Kelvin. For homogeneous isothermal surfaces T equals thermodynamic temperature.

7.1.2 Radiometric temperature of isothermal surfaces

For a sensor located near the surface and measuring within an atmospheric TIR window the atmospheric influence on the surface-leaving radiance along its path can be neglected. With known emissivity, the simplified radiative transfer equation (Dash *et al.*, 2002) can be used to account for reflected down-welling TIR radiance from the atmosphere and for the non-black body behavior of the surface. The blackbody equivalent spectral radiance B emitted by the surface at temperature T is given by:

$$B(T,\lambda) = \frac{R(T,\lambda) - \left(1-\varepsilon(\lambda)\right)\cdot R_{sky}(\lambda)}{\varepsilon(\lambda)} \qquad \text{B.2}$$

where R is the measured surface-leaving spectral radiance and R_{sky} is the measured down-welling hemispherical sky radiance. In situ measurements of R_{sky} are usually performed by a dedicated radiometer aligned at the zenith angle of about 53° (Kondratyev, 1969; Sakai *et al.*, 2009; Göttsche *et al.*, 2016), which depends slightly on spectral band and atmospheric conditions, or via a known relationship between the radiance measured at zenith and hemispherical radiance (Rubio *et al.*, 1997). Once the blackbody equivalent spectral radiance B is known, inverting Planck's law gives the 'radiometric temperature' T of the surface. The spectral response functions of many radiometers are approximately symmetric, while Planck's function and the spectral emissivity of natural surfaces generally vary slowly over a 'narrow band' radiometer's spectral range. Therefore, LST is usually retrieved by evaluating Planck's function at the radiometer's centre wavelength (Goettsche and Hulley, 2012).

7.1.3 Radiometric temperature of non-isothermal surfaces

A single well-calibrated radiometer can be sufficient to obtain representative in situ LST for homogeneous sites (Göttsche *et al.*, 2013). However, natural surfaces are rarely homogenous and isothermal at a given pixel size. Therefore, heterogeneous sites require at least one radiometer for each of the site's endmembers, which have to be sufficiently homogeneous and their relative area fractions have to be known (Guillevic *et al.*, 2013; Ermida *et al.*, 2014). Furthermore, the definitions given in section 7.1.2 for homogeneous isothermal surfaces have to be re-expressed in terms of end-member fractions and their respective emissivities. Following (Becker and Li, 1995), for a flat surface consisting of N homogeneous and isothermal sub-elements having normalised fractional areas S_k we obtain

$$\langle\varepsilon\rangle_\lambda = \sum_{k=1}^{N} \varepsilon_{\lambda k}\, S_k \qquad \text{B.3}$$

$$\langle T\rangle_\lambda = B_\lambda^{-1}\left[\frac{\sum_{k=1}^{N} \varepsilon_{\lambda k}\, B_\lambda(T_k) S_k}{\langle\varepsilon\rangle_\lambda}\right] \qquad \text{B.4}$$

The definition of 'radiometric temperature' given by equation B.4 is scale-invariant and in the 10-12 µm band leads to very similar values as the alternative definition of 'radiative temperature'; for a more in-depth treatment on temperature definitions for non-isothermal heterogeneous surface please refer to (Becker and Li, 1995).

7.2 Emissivity

It is obvious from section 7.1 that accurate information about surface emissivity must be available for converting brightness temperature (BT) measurements into accurate in situ LST. Emissivity can be obtained from in situ measurements (Rubio *et al.*, 1997) or from spectral libraries (Baldridge *et al.*, 2009). Whereas for spatially and temporally homogeneous field sites, e.g. lakes or dense rice fields, it can be sufficient to provide a single emissivity value, heterogeneous sites require an emissivity estimate for each endmember. In addition, some sites might exhibit phenology-dependent emissivity values or emissivity changes with surface moisture. For deriving accurate in situ LST it is essential that the estimated emissivity is representative of the observed endmembers at the time of the BT measurements.

Comparing broadband emissivities in the 8-12 µm range obtained from the Advanced Spaceborne Thermal Emission and Reflection Radiometer (ASTER) and from the Moderate Resolution Imaging Spectroradiometer (MODIS), Ogawa *et al.* (2008) found that LSE over arid regions varies over a wide range of 0.86 to 0.96. ASTER spectral library (Baldridge *et al.*, 2009) data for rocks, soils, and sand, which are frequently encountered components of land covers in (semi-)arid regions, typically show emissivity variations of about ±0.04 about their mean over the 8 - 12 µm spectral range; in contrast, for completely vegetated surfaces the corresponding LSE variations are typically ±0.01.

7.2.1 In situ emissivity

While channel-effective in situ emissivities can be determined with the 'emissivity box method' in the field (Rubio *et al.*, 1997), spectral emissivities are usually obtained for samples in the laboratory (Salisbury and D'Aria, 1992). For sites consisting of well-known static endmembers it may also be feasible to use representative values from spectral emissivity libraries, e.g. Baldridge *et al.* (2009), or from literature. However, in case in situ emissivity is not well known and/or suspected to change over time, e.g. due to vegetation cycles, it may be advisable to use a dynamic emissivity estimate derived from satellite observations instead, e.g. as provided by the monthly 'ASTER Global Emissivity Dataset' (GEDv4) at 5 km spatial resolution (Hulley *et al.*, 2015) or the 1 km MOD21 daily product retrieved from MODIS (Hulley and Hook, 2010).

7.2.2 Emissivity box method

The 'one-lid emissivity box method' is well suited to determine LSE for sufficiently open, relatively flat, and unobstructed field sites with frequent clear sky conditions. Rubio *et al.* (1997) studied the one-lid and the two-lid method in detail and derived correction terms for the two methods. While the 'two-lid emissivity box method' is independent of sky conditions (Sobrino and Caselles, 1993), it is technically more demanding and requires an isothermally heated lid with near unit emissivity. Therefore, we recommend the one-lid emissivity box method, which consists of the sequence of radiance measurements shown in Figure

B.1 and an additional measurement of sky radiance.

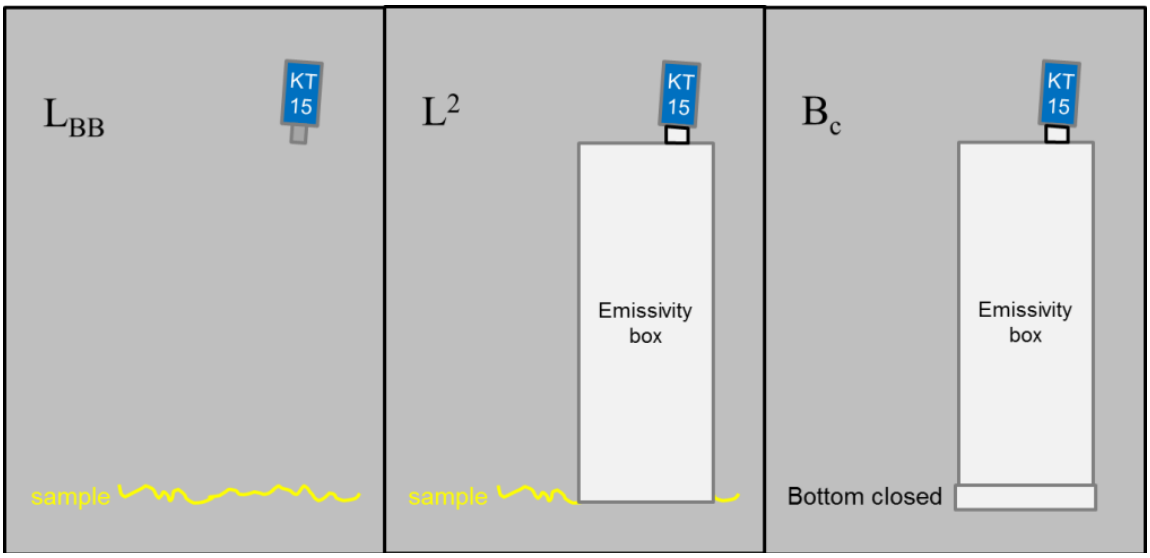

Figure B.1. Radiance measurements performed for the one-lid emissivity box method (KT15 radiometer).

Using the same nomenclature as (Rubio *et al.*, 1997), uncorrected LSE ε_0 is obtained from a sequence of three radiance measurements (see Figure B.1):

$$\varepsilon_0 = \frac{L_{BB} - L_a^{\downarrow}}{L^2 - L_a^{\downarrow}} \qquad \text{B.5}$$

where L_{BB} is the sample radiance measured under clear sky conditions (i.e. without the box), $L_a^{\downarrow}$ is the downwelling sky radiance, and L^2 is the radiance measured through the bottomless box when it is placed on the sample. Corrected LSE is then given by:

$$\varepsilon = \varepsilon_0 + \delta\varepsilon \qquad \text{B.6}$$

with correction

$$\delta\varepsilon = (1 - \varepsilon_0)\left\{1 - \frac{L^2 - L_a^{\downarrow}}{L^2 - L_a^{\downarrow} - R(L^2 - B_c)}\right\} \qquad \text{B.7}$$

where R is a box-specific factor, which depends on box geometry and the spectral response of the inner walls. For box dimensions of 30 cm x 30 cm x 80 cm and an emissivity of $\varepsilon_c = 0.03$ for highly polished aluminum Rubio *et al.* (1997) obtained $R = 0.265$. The term B_c is the radiance measured through the box when its bottom is closed with a sheet of aluminum, i.e. it corresponds to the temperature of the 'cold' aluminum. In order to avoid the 'narcissus' effect, i.e. the radiometer observing its own reflection, the opening in the top of the emissivity box can be slightly off-centre so that the inserted radiometer is inclined

by 5° w.r.t. nadir (Goettsche and Hulley, 2012).

Down-welling hemispherical sky radiance $L_a^{\downarrow}$ is usually approximated with the radiance measured at the 'representative' zenith angle of about 53° (Kondratyev, 1969; Coll *et al.*, 2005) or estimated as

$$L_a^{\downarrow} = 1.3 \times B[T(0^{\circ})] \qquad \text{B.8}$$

where B is the Planck function evaluated at the radiometer's centre wavelength and $T(0^{\circ})$ is brightness temperature measured at zenith (Rubio *et al.*, 1997).

The larger the difference between clear sky brightness temperature and surface temperature, the higher the signal to noise ratio of the box method and the smaller the emissivity correction $\delta\varepsilon$. The box method assumes that the temperature of the sample remains (approximately) constant between the measurements over the sample (Figure B.1, left and center), which requires quick handling of the box and fast readings. Goettsche and Hulley (2012) recorded brightness temperatures automatically once per second, which also allows choosing the optimum measurements in terms of thermal stability 'off-line'.

7.3 Best practices for obtaining in situ LST

In situ LST is not directly measured but derived from measurements of surface brightness temperature (BT), sky BT and land surface emissivity (LSE). However, in situ observations of LST taken under the right conditions over large and homogeneous sites currently allow the most accurate validation of LST products ('Category A validation'; Schneider *et al.*, 2012). For in situ LST to be representative over a large range of spatial scales, i.e. from the ground-based radiometer's GIFOV to the satellite pixel scale, a field site needs to be either homogeneous over all relevant scales or it must be possible to obtain a representative LST by combining radiance measurements performed over a few 'endmembers', e.g. via equation B.4 or by modelling (Pinheiro *et al.*, 2004; Guillevic *et al.*, 2013; Ermida *et al.*, 2014). The homogeneity of a site can be assessed by studying its spatial LST variability (standard deviation) with ground-based radiometers (Wan *et al.*, 2002; Coll *et al.*, 2009b) or by analyzing high-resolution TIR imagery (e.g. from ASTER; GIFOV ≈ 100 m). For the latter (Schneider *et al.*, 2012) recommend a standard deviation of no more than 0.5 K. In situ measurements over rice fields and uniform grasslands yielded a similar spatial variability (Coll *et al.*, 2009b).

7.3.1 Measurement protocol for in situ LST

Measurements with FRM TIR radiometers are often performed to validate satellite-derived LST products; since all satellite data are subject to geolocation error, for validation purposes it is recommended that the sites should be homogenous over at least 3 × 3 pixels. Field campaigns for obtaining in situ LST typically last between a few days and a few weeks and are most often performed over naturally homogenous (and relatively isothermal) sites, e.g. rice fields (Coll *et al.*, 2005; Coll *et al.*, 2009a, Niclos *et al.*, 2011), grasslands (Wan *et al.*, 2002), arid regions (Wan *et al.*, 2002; Goettsche *et al.*, 2013), or agricultural sites (Sobrino *et al.*, 2007): this ensures that the in situ measurements are representative of the immediate surroundings. Here, we propose a measurement protocol for obtaining in-situ LST with a single radiometer placed over a highly homogeneous natural target:

- The radiometer shall be traceably calibrated to ±0.3 K or better against a primary reference blackbody (achievable accuracy depends on radiometer type, expected temperature range and environmental conditions).
- Observed surfaces have to be approximately homogeneous and isothermal on the spatial scale of the radiometer (e.g. about 1.6 m GIFOV Ø over dense rice fields). This can be verified with spatially distributed radiometers, by moving a single radiometer 'quickly' across the site, or by spatial analyses of high-resolution satellite data.
- Surface observations shall be performed at near-nadir view angles (<30°) to minimize differences due to LST anisotropy (Cuenca and Sobrino, 2004; Sobrino and Cuenca, 1999)
- Measurements should not be performed next to obstructions like trees or buildings.
- Down-welling hemispherical sky irradiance has to be measured 'simultaneously' with the surface measurements. This can be achieved with a second identical radiometer (i.e. same FOV and spectral range) or by measuring with the same radiometer at short intervals, e.g. every 3 minutes.
- Favorable conditions for estimating down-welling hemispherical sky irradiance from a single directional radiance measurement are completely clear and skies covered completely by uniform stratus clouds (Rubio *et al.*, 1997).
- Instrument-specific Land Surface Emissivity (LSE) should be determined under favorable environmental conditions, e.g. at night-time for clear sky and low wind speeds; the two-lid emissivity box method works under less favorable conditions.
- All clocks involved in the campaign shall be synchronized to time UTC
- The time of each measurement shall be recorded in UTC and the corresponding geolocation in decimal degrees latitude / longitude
- All data shall recorded in a common table format
- Relevant technical details of each instrument shall be documented, e.g. make & type, serial number, spectral range and calibration details
- Information about wind, cloud-cover, air temperature and humidity, land cover, etc. shall be documented

7.3.2 Down-welling hemispherical sky radiance

Down-welling hemispherical sky irradiance is usually estimated from one of the following measurements performed with the LST FRM field TIR radiometer:

- Sky BT at the 'representative zenith angle' of about 53° (Kondratyev, 1969; Sakai *et al.*, 2009)
- Sky BT at 0° zenith angle and a known relationship (equation B.8; Rubio *et al.*, 1997)
- BT measured over a diffuse gold plate or crinkled aluminum foil (Salisbury 1998)

The first approach directly yields an estimate of down-welling hemispherical sky irradiance for the spectral range of the radiometer, while the second approach is easier to implement in terms of directional alignment. The third approach requires that the reflector's temperature and emissivity spectrum are known. However, since the gold plate and aluminum foil have very high reflectance in the TIR (about 97%), their emitted radiance is a relatively small part of the measured signal (Salisbury, 1998). Garcia-Santos *et al.* (2013) compared four different methods for retrieving hemispherical down-welling irradiance (the three above and radiative transfer calculations for atmospheric profile data): for clear-sky conditions and an unobstructed upper hemisphere the methods produced comparable results. Depending on the spectral range of the radiometer, measured sky BT can be very low, e.g. -100 °C for clear dry atmospheres over deserts when measuring at 0° zenith angle (Salisbury, 1998; Göttsche and Hulley, 2012). Besides potentially exceeding their operating range, radiometers are generally difficult to calibrate for temperatures well below 0 °C, which may result in larger measurement errors. Fortunately, the typically high emissivity of natural land surfaces around 11 µm (e.g. between 0.92 and 0.99) reduces the impact of such errors on derived LST; the effect of emissivity errors is usually considerably more severe (Schädlich *et al.*, 2001).

7.3.3 Land Surface Emissivity

Before in situ LST can be obtained, directional spectral emissivity matching the radiometer has to be estimated; the spatial sampling has to be appropriate to provide representative LSE at all scales of interest, e.g. at the scale of the in situ radiometer and the satellite pixel. In situ emissivities can be estimated with the emissivity box method (section 7.2.2) or from spectroscopic measurements over samples in the laboratory. For some land surface covers, e.g. dense green vegetation, LSE values are well known and may also be obtained from spectral libraries or literature. When obtaining in situ LST, it has to be ensured that the corresponding LSE has remained approximately the same since it was determined (e.g. no change in land cover due to vegetation, fire, etc.).

7.3.4 In situ LST for heterogeneous surfaces

For heterogeneous surfaces consisting of several 'flat' endmembers (i.e. their cover fractions are independent of viewing and illumination geometry) the measurement protocol for homogenous surfaces (section 7.3.1) is applied to each endmember and LST can be obtained using equation B.4. However, this usually requires multiple radiometers since the BT and LSE of each endmember need to be simultaneously available. For non-flat endmembers, e.g. trees, cover fractions need to be projected to the ground for a specific viewing and illumination geometry, e.g. for a satellite at overpass time, so that a matching in situ LST can be obtained. A further complication arises from the associated variable shadow fraction. Therefore, obtaining accurate in situ LST over non-flat ('vertically structured') heterogeneous land surfaces usually requires some modelling (Pinheiro *et al.*, 2004; Guillevic *et al.*, 2013; Ermida *et al.*, 2014) or is limited to night-time.

REFERENCES

Augustine, J. A., DeLuisi, J. J., and Long, C. N. (2000). SURFRAD—A national surface radiation budget network for atmospheric research. Bulletin of the American Meteorological Society, 81, 2341–2357.

Augustine, J. A., Hodges, G. B., Cornwall, C. R., Michalsky, J. J., and Medina, C. I. (2005). An Up- date on SURFRAD—The GCOS Surface Radiation Budget Network for the Continental United States. Journal of Atmospheric and Oceanic Technology, 22, 1460–1472.

Allen, R. G., Tasumi, M., and Trezza, R. (2007). Satellite-based energy balance for mapping evapotranspiration with internalized calibration (METRIC)-model, *Journal of Irrigation and Drainage Engineering*, 133, 380-394.

Anderson, M.C., Norman, J.M., Diak, G.R., Kustas, W.P., & Mecikalski, J.R. (1997). A two-source time-integrated model for estimating surface fluxes using thermal infrared remote sensing. Remote Sens. Environment, 60, 195–216.

Anderson, M. C., C. R. Hain, B. D. Wardlow, A. Pimstein, J. R. Mecikalski and W. P. Kustas, (2011a). Evaluation of drought indices based on thermal remote sensing of evapotranspiration over the continental United States. Journal of Climate, 24, 2025-2044.

Anderson, M. C., Allen, R.G., Morse, A., & Kustas, W.P. (2012). Use of Landsat thermal imagery in monitoring evapotranspiration and managing water resources. Remote Sens. Environ., 122, 50-65.

Anderson, M.C., Kustas, W.P., Norman, J.M., Hain, C.R., Mecikalski, J.R., Schultz, L., Gonzalez-Dugo, M.P., Cammalleri, C., d'Urso, G., Pimstein, A., and Gao, F. (2011b). Mapping daily evapotranspiration at field to continental scales using geostationary and polar orbiting satellite imagery. Hydrology and Earth System Sciences, 15, 223-239.

Anderson, M.C., Hain, C.R., Jurecka, F., Trnka, M., Hlavinka, P., Dulaney, W., Otkin, J.A., Johnson, D., and Gao, F. (2016a). Relationships between the evaporative stress index and winter wheat and spring barley yield anomalies in the Czech Republic. Climate Research, 70, 215-230.

Anderson, M.C., Zolin, C.A., Sentelhas, P.C., Hain, C.R., Semmens, K., Yilmaz, M.T., Gao, F., Otkin, J.A., and Tetrault, R. (2016b). The Evaporative Stress Index as an indicator of agricultural drought in Brazil: An assessment based on crop yield impacts. Remote Sensing of Environment, 174, 82-99.

Baldridge, A.M., Hook, S.J., Grove, C.I., Rivera, G. (2009). The ASTER spectral library version 2.0. Remote Sensing of Environment 113, 711-715.

Barbosa, P.M., Pereira, J.M.C., and Gegoire, J.-M. (1998). Compositing Criteria for Burned Area Assessment Using Multitemporal Low Resolution Satellite Data. Remote Sensing of Environment, Vol. 65, pp. 38–49.

Barsi, J. A., Schott, J.R., Palluconi, F.D., Helder, D.L., Markham, B.L., Chander, G., and O'Donnell, E.M. (2003). Landsat TM and ETM+ Thermal Band Calibration, Canadian Journal of Remote Sensing, Vol. 29, No. 2 pp. 141-153.

Barsi, J.A., Hook, S.J., Schott, J.R., Raqueno, N.G., Markham, B.L. (2007). Landsat 5 Thematic Mapper Thermal Band Calibration Update, IEEE Geoscience and Remote Sensing Letters, Vol. 4, Number 4, pp. 552-555.

Barsi, J. A., Schott, J. R., Hook, S. J., Raqueno, N. G. Markham, B. L., and Radocinski, R. G. (2014). Landsat-8 Thermal Infrared Sensor (TIRS) vicarious Radiometric Calibration. Remote Sensing, 6, pp. 11607-11626, doi:10.3390/rs61111607.

Basist, A., Grody, N.C., Peterson, T.C., and Williams, C.N. (1998). Using the Special Sensor Microwave/Imager to Monitor Land Surface Temperatures, Wetness, and Snow Cover. Journal of Applied Meteorology, Vol.37, pp. 888-911.

Becker, F., and Li, Z.-L. (1995). Surface temperature and emissivity at various scales: definition, measurement and related problems. Remote Sensing Reviews, 12(3-4):225–253.

Belward, A.S. (1996). The IGBP-DIS global 1 km land cover data set (DISCover)—Proposal and implementation plans. IGBP-DIS Office, Toulouse, France. IGBP-DIS working paper 13.

Cao, C., Weinreb, M. and Xu, H. (2004). Predicting simultaneous nadir overpasses among polar-orbiting meteorological satellites for the intersatellite calibration of radiometers. Journal of Atmospheric and Oceanic Technology, 21:4 537-542.

Caselles, V. and Sobrino, J.A. (1989). Determination of frosts in orange groves from NOAA-9 AVHRR data. Remote Sensing of Environment, vol. 29, no. 2, 135–146.

Cleugh, H.A., Leuning, R., Mu, Q., and Running, S.W. (2007). Regional evaporation estimates from flux tower and MODIS satellite data. Remote Sensing of Environment, Vol. 106, pp. 285–304.

Coll, C., Caselles, V., Galve, J. M., Valor, E., Niclós, R., Sanchez, J. M., *et al.* (2005). Ground measurements for the validation of land surface temperatures derived from AATSR and MODIS data. Remote Sensing of Environment, 97, 288–300.

Coll, C., Hook, S. J., and Galve, J. M. (2009a). Land surface temperature from the advanced Along-Track Scanning Radiometer: Validation over inland waters and vegetated surfaces. IEEE Transactions on Geoscience and Remote Sensing, 47, 350–360.

Coll, C., Wan, Z., and Galve, J. M. (2009b). Temperature-based and radiance-based validations of the V5 MODIS land surface temperature product. Journal of Geophysical Research, [Atmospheres], 114, D20102, http://dx.doi.org/10.1029/2009JD012038.

Coll, C., Galve, J. M., Sanchez, J. M., and Caselles, V. (2010). Validation of Landsat-7/ETM+ thermal-band calibration and atmospheric correction with ground-based measurements. IEEE Transactions on Geoscience and Remote Sensing, 48, 547–555.

Cuenca, J., and Sobrino, J.A. (2004). Experimental measurements for studying angular and spectral variation of thermal infrared emissivity. Applied Optics, 43(23):4598–4602.

Da Silva, J. R. M., Damasio, C. V., Sousa, A. M. O., Bugalho, L., Pessanha, L., Quaresma, P. (2015). Agriculture pest and disease risk maps considering MSG satellite data and land surface temperature, Int. J. App Earth Observation Geoinformation, 38, 40-50, doi: 10.1016/j.jag.2014.12.016

Dash, P., Göttsche, F.-M., Olesen, F.-S., and Fischer, H. (2002). Land surface temperature and emissivity estimation from passive sensor data: theory and practice-current trends. International Journal of Remote Sensing, 23(13):2563–2594.

Dee, D.P., Uppala, S.M., Simmons, A.J., Berrisford, P., Poli, P., Kobayashi, S., Andrae, U., Balmaseda, M.A., Balsamo, G., Bauer, P., Bechtold, P., *et al.* (2011). The ERA-Interim reanalysis: configuration and performance of the data assimilation system. Quarterly Journal of the Royal Meteorological Society 137, 553-597.

Diamond, H. J., T. R. Karl, M. A. Palecki, C. B. Baker, J. E. Bell, R. D. Leeper, D. R. Easterling, J. H. Lawrimore, T. P. Meyers, M. R. Helfert, G. Goodge, and P. W. Thorne (2013). U.S. Climate Reference Network after one decade of operations: status and assessment. Bull. Amer. Meteor. Soc., 94, 489-498. doi: 10.1175/BAMS-D-12-00170.1

Dousset, B., and Gourmelon, F. (2003). Satellite multi-sensor data analysis of urban surface temperatures and landcover. Isprs Journal of Photogrammetry and Remote Sensing, 58, 43-54.

Dousset, B., Gourmelon, F., Laaidi, K., Zeghnoun, A., Giraudet, E., Bretin, P., Mauri, E., and Vandentorren, S. (2011). Satellite monitoring of summer heat waves in the Paris metropolitan area. International Journal of Climatology, 31, 313-323.

Ermida, S.L., Trigo, I.F., DaCamara, C.C., Göttsche, F.-M., Olesen, F.-S. and Hulley, G. (2014). Validation of remotely sensed surface temperature over an oak woodland landscape—The problem of viewing and illumination geometries. Remote Sensing of Environment, 148, 16-27.

Ermida, S.L., DaCamara, C. C., Trigo, I. F., Pires, A. C., Ghent, D., Remedios, J. (2017a). Modelling directional effects on remotely sensed land surface temperature. Remote Sens. Env., 190, 56-69. doi: 10.1016/j.rse.2016.12.008

Ermida, S.L., Jimenez, C., Prigent, C., Trigo, I. F. and DaCamara, C. C. (2017). Inversion of AMSR-E observations for land surface temperature estimation - Part 2: Global comparison with infrared satellite temperature, J. Geophys. Res.,DOI: 10.1002/2016JD026148.

Fernandes, R., Plummer, S., Nightingale, J., Baret, F., Camacho, F., Fang, H., Garrigues, S., Gobron, N., Lang, M., Lacaze, R., LeBlanc, S., Meroni, M., Martinez, B., Nilson, T., Pinty, B., Pisek, J., Sonnentag, O., Verger, A., Welles, J., Weiss, M., & Widlowski, J.L. (2014). Global Leaf Area Index Product Validation Good Practices. Version 2.0. In G. Schaepman-Strub, M. Román, & J. Nickeson (Eds.), Best Practice for Satellite-Derived Land Product Validation (p. 76): Land Product Validation Subgroup (WGCV/CEOS), doi:10.5067/doc/ceoswgcv/lpv/lai.002

Fisher, J. B., K. P. Tu, and D. D. Baldocchi (2008). Global estimates of the land-atmosphere water flux based on monthly AVHRR and ISLSCP-II data, validated at 16 FLUXNET sites. Remote Sensing of Environment, 112(3), 901–919, doi:10.1016/j.rse.2007.06.025.

Freitas, S.C., Trigo, I.F., Bioucas-Dias, J.M., and Göttsche, F.-M. (2010). Quantifying the Uncertainty of Land Surface Temperature Retrievals From SEVIRI/Meteosat. IEEE Transactions on Geoscience and Remote Sensing, 48(1), 523-534.

Gallego-Elvira B., Olioso A., Mira M., Reyes- Castilloa, S., Boulet, G., *et al.*, 2013. EVASPA (EVApotranspiration Assessment from SPAce) tool: An overview. *Procedia Environmental Sciences*, 19, 303–310.

Garcia-Haro, F. J., Sommer, S. and Kemper, T. (2005). Variable multiple endmember spectral mixture analysis (VMESMA). International Journal of Remote Sensing, vol. 26, no. 10, 2135–2162.

Garcia-Santos, V., Valor, E., Caselles, V., Mira, M., Galve, J.M. and Coll, C. (2013). Evaluation of Different Methods to Retrieve the Hemispherical Downwelling Irradiance in the Thermal Infrared Region for Field Measurements. IEEE Transactions on Geoscience and Remote Sensing, 51(4), 2155–2165.

GCOS-82, the Second Report on the Adequacy of the Global Observing Systems for Climate in Support of the UNFCCC, GCOS-82, April 2003 (WMO/TD No. 1143).

GCOS-200. The Global Observing System for Climate: Implementation Needs, 342PP. WMO, 2016. (available at https://library.wmo.int/opac/doc_num.php?explnum_id=3417)

Gillespie, A., Rokugawa, S., Matsunaga, T., Cothern, J. S., Hook, S. and Kahle, A. B. (1998). A temperature and emissivity separation algorithm for Advanced Spaceborne Thermal Emission and Reflection Radiometer (ASTER) images. *IEEE Transactions on Geoscience and Remote Sensing*, 36(4), 1113-1126, doi: 10.1109/36.700995.

Göttsche, F., Olesen, F. S., Hoyer, J. L., Wimmer, W., and Nightingale, T. (2017). Fiducial Reference Measurements for Validation of Surface Temperature from Satellites (FRM4STS) Technical Report TR-3: A framework to verify the field performance of TIR FRM. Reference OFE-D-120-V1-Iss-3-Ver-1-ISSUED, 75 pages.

Göttsche, F.-M., Olesen, F.-S., Trigo, I., Bork-Unkelbach, A., and Martin, M. (2016). Long Term Validation of Land Surface Temperature Retrieved from MSG/SEVIRI with Continuous in-Situ Measurements in Africa. Remote Sensing, 8, 410.

Goettsche, F. -M., Olesen, F. -S., and Bork-Unkelbach, A. (2013). Validation of land surface temperature derived from MSG/SEVIRI with in situ measurements at Gobabeb, Namibia. International Journal of Remote Sensing, 34(9–10), 3069–3083.

Goettsche, F. -M., and Hulley, G. C. (2012). Validation of six satellite-retrieved land surface emissivity products over two land cover types in a hyper-arid region. Remote Sensing of Environment, 124, 149–158.

Guillevic, P., Gastellu-Etchegorry, J. P., Demarty, J., and Prevot, L. (2003). Thermal infrared radiative transfer within three-dimensional vegetation covers. Journal of Geophysical Research, [Atmospheres], 108, 4248.

Guillevic, P. C., Privette, J. L., Coudert, B., Palecki, M.A., Demarty, J., Ottlé, C., *et al.* (2012). Land Surface Temperature product validation using NOAA's surface climate observation networks - Scaling methodology for the Visible Infrared Imager Radiometer Suite (VIIRS). Remote Sensing of Environment, 124, 282–298, http://dx.doi.org/10. 1016/j.rse.2012.05.004.

Guillevic, P. C., Bork-Unkelbach, A., Göttsche, F. M., Hulley, G. C., Gastellu-Etchegorry, J. -P., Olesen, F. S., *et al.* (2013). Directional viewing effects on satellite Land Surface Temperature products over sparse vegetation canopies—A multisensor analysis. IEEE Geoscience and Remote Sensing Letters, 99, 1–5, http://dx.doi.org/10.1109/LGRS. 2013.2260319.

Guillevic, P. C., Biard, J., Hulley, G. C., Privette, J. L., Hook, S. J., Olioso, A., Göttsche, F.-M., Radocinski, R., Román, M. O., Yu, Y., and Csiszar I. (2014). Validation of Land Surface Temperature products derived from the Visible Infrared Imager Radiometer Suite (VIIRS) using ground-based and heritage satellite measurements. Remote Sensing of Environment, 154 (2014) 19–37, doi: 10.1016/j.rse.2014.08.013.

GUM-2008, Evaluation of measurement data — Guide to the expression of uncertainty in measurement, Joint Committee for Guides in Metrology (JCGM 100:2008, GUM 1995 with minor corrections), September 2008, http://www.bipm.org/utils/common/documents/jcgm/JCGM_100_2008_E.pdf.

Hain, C.R., Crow, W.T., Mecikalski, J.R., Anderson, M.C., and Holmes, T. (2011). An intercomparison of available soil moisture estimates from thermal infrared and passive microwave remote sensing and land surface modeling. Journal of Geophysical Research-Atmospheres, 116, D15107.

Hall, A., and Jones, G.V. (2010). Spatial analysis of climate in wine grape-growing regions in Australia. Australian Journal of Grape and Wine Research, 16, 389-404.

Hall, D.K., Comiso, J.C., DiGirolamo, N.E., Shuman, C.A., Key, J.R., and Koenig, L.S. (2012). A Satellite-Derived Climate-Quality Data Record of the Clear-Sky Surface Temperature of the Greenland Ice Sheet. Journal of Climate, 25, 4785-4798.

Hook, S. J., G. Chander, J. A. Barsi, R. E. Alley, A. Abtahi, F. D. Palluconi, B. L. Markham, R. C. Richards, S. G. Schladow, and D. L. Helder (2004). In-Flight Validation and Recovery of Water Surface Temperature with Landsat 5 Thermal Infrared Data Using an Automated High Altitude Lake Validation Site at Lake Tahoe CA/NV, USA. IEEE Transactions Geoscience and Remote Sensing, vol. 42, pp. 2767- 2776, 2004.

Hook, S. J., W. B. Clodius, L. Balick, R. E. Alley, A. Abtahi, R. C. Richards, and S. G. Schladow (2005). In-Flight Validation of Mid- and Thermal Infrared Data from the Multispectral Thermal Imager (MTI) Using an Automated High-Altitude Validation Site at Lake Tahoe CA/NV, USA. IEEE Transactions Geoscience and Remote Sensing, vol. 43, pp. 1991- 1999.

Hook, S. J., Vaughan, R. G., Tonooka, H., and Schladow, S. G. (2007). Absolute radiometric in-flight validation of mid infrared and thermal infrared data from ASTER and MODIS on the Terra spacecraft using the Lake Tahoe, CA/NV, USA, automated validation site. IEEE Transactions on Geoscience and Remote Sensing, 45, 1798–1807.

Hulley, G. C., & Hook, S. J. (2009a). Intercomparison of versions 4, 4.1 and 5 of the MODIS Land Surface Temperature and emissivity products and validation with laboratory measurements of sand samples from the Namib Desert, Namibia. Remote Sensing of Environment, 133, 1313–1318.

Hulley, G. C., and Hook, S. J. (2009b). The North American ASTER Land Surface Emissivity Database (NAALSED) Version 2.0. Remote Sensing of Environment, 1967–1975.

Hulley, G. C., and Hook, S. J. (2010). Generating consistent Land Surface Temperature and emissivity products between ASTER and MODIS data for earth science research. IEEE Transactions on Geoscience and Remote Sensing, 1304–1315, http://dx.doi.org/ 10.1109/TGRS.2010.2063034.

Hulley, G. C., Hook, S. J., and Schneider, P. (2011). Optimized split-window coefficients for deriving surface temperatures from inland water bodies. Remote Sensing of Environment, 115, 3758–3769.

Hulley, G. C., Hughes, C. G., and Hook, S. J. (2012). Quantifying uncertainties in land surface temperature and emissivity retrievals from ASTER and MODIS thermal infrared data. *Journal of Geophysical Research-Atmospheres*, vol 117, pp. D23113- D23130.

Hulley, G., Veraverbeke, S., and Hook, S. (2014). Thermal-based techniques for land cover change detection using a new dynamic MODIS multispectral emissivity product (MOD21). Remote Sensing of Environment, 140, 755-765.

Hulley, G.C., Hook, S.J., Abbott, E., Malakar, N., Islam, T., and Abrams, M. (2015). The ASTER global emissivity dataset (ASTER GED): Mapping earths emissivity at 100 meter spatial scale. Geophys. Res. Lett., 42(19):7966–7976.

Islam I., Hulley, G. C., Malakar, N. K., Radocinski, R. G., Hook, S. J. and Guillevic, P. C. (2017). A physics-based algorithm for the simultaneous retrieval of land surface temperature and emissivity from VIIRS thermal infrared data, IEEE Transactions on Geoscience and Remote Sensing, 55, 1, 563-576.

Jacob, F., Petitcolin, F., Schmugge, T., Vermote, E., French, A., and Ogawa, K. (2004). Comparison of land surface emissivity and radiometric temperature derived from MODIS and ASTER sensors. Remote Sensing of Environment, 90, 137–152.

Jedlovec, G.J. Haines, S.L., and LaFontaine, F.J. (2008). Spatial and Temporal Varying Thresholds for Cloud Detection in GOES Imagery. IEEE Transactions on Geoscience and Remote Sensing, V. 46, N. 6, 1705-1717.

Jimenez, C., Prigent, C., Ermida, S. L. and Moncet, J.-L. (2017) Inversion of AMSR-E observations for land surface temperature estimation - Part 1: Methodology and evaluation with station temperature, J. Geophys. Res. DOI: 10.1002/2016JD026144.

Jiménez-Muñoz, J.C., and Sobrino, J.A. (2007). Emissivity spectra obtained from field and laboratory measurements using the temperature and emissivity separation algorithm. Applied Optics, 45, 7104–7109.

Jones, G.V., Duff, A.A., Hall, A., and Myers, J.W. (2010). Spatial Analysis of Climate in Winegrape Growing Regions in the Western United States. American Journal of Enology and Viticulture, 61, 313-326.

Kalma, J.D., McVicar, T.R., and McCabe, M.F. (2008). Estimating Land Surface Evaporation: A Review of Methods Using Remotely Sensed Surface Temperature Data. Surv Geophys, Vol.29, pp.421–469.

Kalnay, E., Kanamitsu, M., Kistler, R., Collins, W., 1996. The NCEP/NCAR 40-year reanalysis project. Bulletin of the American Meteorological Society 77, 437-471.

Kealy, P.S., and Hook, S. (1993). Separating temperature & emissivity in thermal infrared multispectral scanner data: Implication for recovering land surface temperatures. IEEE Transactions on Geoscience and Remote Sensing, 31, 1155-1164.

Kogan, F.N. (1995). Application of vegetation index and brightness temperature for drought detection. Advances in Space Research, 15(11), 91–100.

Kogan, F.N. (1997). Global drought watch from space. Bulletin of the American Meteorological Society, 78(4), 621–636.

Kondratyev, K. Y., (1969). Radiation in the Atmosphere. International geophysics series, vol. 12, New York, NY; London: Academic Press.

Korb, A. R., Salisbury, J. W., and D'Aria, D. M. (1999). Thermal-infrared remote sensing and Kirchhoff's law 2. Field measurements. *Journal of Geophysical Research-Solid Earth*, 104(B7), 15339–15350.

Krehbiel, C., and Henebry, G.M. (2016). A Comparison of Multiple Datasets for Monitoring Thermal Time in Urban Areas over the US Upper Midwest. Remote Sensing, 8(4), 297; doi:10.3390/rs8040297.

Lambin, E.F., and Ehrlich, D. (1997). Land-cover Changes in Sub-Saharan Africa (1982-1991): Application of a Change Index Based on Remotely Sensed Surface Temperature and Vegetation Indices at a Continental Scale. Remote Sensing of Environment, Vol.61, pp. 181–200.

Li, Z. -L., Tang, B. H., Wu, H., Ren, H. Z., Yan, G. J., Wan, Z. M., *et al.* (2013). Satellite-derived land surface temperature: Current status and perspectives. Remote Sensing of Environment, 131, 14–37, http://dx.doi.org/10.1016/j.rse.2012.12.008.

Li, H., Sun, D., Yu, Y., Wang, H., Liu, Y., Liu, Q., *et al.* (2014). Evaluation of the VIIRS and MODIS LST products in an arid area of Northwest China. Remote Sensing of Environment, 142, 111–121, http://dx.doi.org/10.1016/j.rse.2013.11.014.

Llewellyn-Jones, D., Edwards, M., Mutlow, C., Birks, A., Barton, I., Tait, H., 2001. AATSR: global-change and surface-temperature measurements from ENVISAT. ESA bulletin 105, 10–21.

Luvall, J., Quattrochi, D.A., Rickman, D., and Estes, M.G. (Eds.) (2015). Urban Heat Islands: Encyclopedia of Atmospheric Sciences.

Malakar, N., and Hulley, G. (2016). A Case Study of Warming Trends and Spatial Patterns of Land Surface Temperatures over the Greater Los Angeles Area Using a new MODIS LST product In, American Geophysical Union (AGU). San Francisco, CA.

Martin, M. A., and Göttsche, F.-M. (2016). Satellite LST Validation Report (DEL-13). ESA DUE GlobTemperature Project, reference GlobT-WP4-DEL-12, www.globtemperature.info.

Martin, M. A., Göttsche, F.-M., Ghent, D., Trent, T., Dodd, E., Pires, A., Trigo, I., Prigent, C. and Jimenez, C. (2016). Satellite LST Intercomparison Report (DEL-13). ESA DUE GlobTemperature Project, reference GlobT-WP4-DEL-13, www.globtemperature.info.

Matricardi, M. (2009). Technical Note: An assessment of the accuracy of the RTTOV fast radiative transfer model using IASI data. Atmospheric Chemistry and Physics, 9, 6899-6913.

Matsunaga, T. (1994). A temperature-emissivity separation method using an empirical relationship between the mean, the maximum, & the minimum of the thermal infrared emissivity spectrum, in Japanese with English abstract. Journal Remote Sensing Society Japan, 14, 230-241.

Merchant, C. J., Matthiesen, S., Rayner, N. A., Remedios, J. J., Jones, P. D., Olesen, F., *et al.* (2013). The surface temperatures of Earth: Steps towards integrated understanding of variability and change. Geoscientific Instrumentation Methods and Data Systems, 2(305–321), 2013, http://dx.doi.org/10.5194/gi-2-305-2013.

Mildrexler, D.J., Zhao, M., Heinsch, F.A., and Running, S.W. (2007). A new satellite-based methodology for continental-scale disturbance detection. Ecological Applications, V.17, pp. 235–250.

Mu, Q., Zhao, M., Kimball, J. S., McDowell, N. G., and Running, S. W. (2013). A Remotely Sensed Global Terrestrial Drought Severity Index. Bulletin of the American Meteorological Society, 01/2013, Vol. 94, Issue 1, Number 1, 83-98, DOI:10.1175/BAMS-D-11-00213.1.

Neteler, M. (2005). Time Series Processing of MODIS Satellite Data for Landscape Epidemiological Applications. International Journal of Geoinformatics, Vol.1, No.1, ISSN 1686–6576.

Neteler, M., Roiz, D., Rocchini, D., Castellani, C., and Rizzoli, A. (2011). Terra and Aqua satellites track tiger mosquito invasion: modelling the potential distribution of Aedes albopictus in north-eastern Italy. International Journal of Health Geographics, 10.

Niclòs, R., Galve, J.M., Valiente, J.A., Estrela, M.J., Coll, C., 2011. Accuracy assessment of land surface temperature retrievals from MSG2-SEVIRI data. Remote Sensing of Environment 115, 2126-2140.

Nishida, K., Nemani, R.R., Running, S.W., and Glassy, J.M. (2003). An operational remote sensing algorithm of land surface evaporation. Journal of Geophysical Research, Vol.108, No. D9, 4270

Norman, G., and Becker, F. (1995). Terminology in thermal infrared remote sensing of natural surfaces. Agricultural and Forest Meteorology, Volume: 77, Issue: 3-4, Pages: 153-166, DOI: 10.1016/0168-1923(95)02259-Z.

Ogawa, K., Schmugge, T., and Rokugawa, S. (2008). Estimating broadband emissivity of arid regions and its seasonal variations using thermal infrared remote sensing. IEEE Transactions on Geoscience and Remote Sensing, 46(2):334–343.

Ouyang, X., Chen, D., Duan, S.-B., Lei, Y., Dou, Y., and Hu, G. (2017). Validation and Analysis of Long-Term AATSR Land Surface Temperature Product in the Heihe River Basin, China. Remote Sensing, 9(152), 1-18, doi:10.3390/rs9020152.

Orth, R., Dutra, E., Trigo, I. F. and Balsamo, G. (2017). Advancing land surface model development with satellite-based Earth observations, Hydrol. Earth Syst. Sci., 21, 2483–2495, Doi: 10.5194/hess-21-2483-2017.

Pasotti, L., Maroli, M., Giannetto, S., and Brianti, E. (2006). Agrometeorology and models for the parasite cycle forecast. Parassitologia, 48, 81-83.

Pinheiro, A.C.T., Privette, J.L., Mahoney, R., and Tucker, C.J. (2004). Directional effects in a daily AVHRR land surface temperature dataset over Africa. IEEE Transactions on Geoscience and Remote Sensing, 42(9):1941–1953.

Pinheiro, A.C.T., Privette, J. L., and Guillevic, P. (2006). Modeling the observed angular anisotropy of land surface temperature in a savanna. IEEE Transactions on Geoscience and Remote Sensing, 44(4), 1036–1047 (April 2006).

Peres, L.F. and DaCamara, C.C. (2005). Emissivity maps to retrieve land-surface temperature from MSG/SEVIRI. IEEE Transactions on Geoscience and Remote Sensing, vol. 43, no. 8, 1834–1844.

Peres, L.F., Libonati, R., and DaCamara, C.C. (2014). Land-Surface Emissivity Retrieval in MSG–SEVIRI TIR Channels Using MODIS Data. IEEE Transactions on Geoscience and Remote Sensing, vol. 52, no.9, 5587–5600.

Prata, A. J. (1994). Land surface temperatures derived from the advanced very high resolution radiometer and the along-track scanning radiometer: 2. Experimental results and validation of AVHRR algorithms. Journal of Geophysical Research: Atmospheres, 99(D6), 13025–13058.

Prata, F., 2002. Land surface temperature measurement from space: AATSR algorithm theoretical basis document. CSIRO Atmospheric Research, Aspendale, Australia.

Randolph, S., Green, R., Peacey, M. and Rogers, D., (2000). Seasonal synchrony: The key to tick-borne encephalitis foci identified by satellite data. Parasitology, Vol. 121, pp. 15–23.

Rasmussen, M.O., Gottsche, F.M., Olesen, F.S., and Sandholt, I. (2011). Directional effects on land surface temperature estimation from Meteosat Second Generation for savanna landscapes IEEE Transactions on Geoscience and Remote Sensing 49 (11), 4458-4468.

Remedios, J. (2012). SLSTR ATBD Land Surface Temperature, Sentinel-3 Optical Products and Algorithm Definition, Version 2.3, ref. S3-L2-SD-03-T03-ULNILU-ATBD_L2LST, Oct. 10, 2012, https://sentinel.esa.int/documents/247904/349589/SLSTR_Level-2_LST_ATBD.pdf.

Rienecker, M. R., Suarez, M. J., Gelaro, R., Todling, R., Bacmeister, J., Liu, E., Bosilovich, M. G., Schubert, S. D. *et al.*, (2011) MERRA: NASA's Modern-Era Retrospective Analysis for Research and Applications. Journal of Climate, 24, 3624–3648, doi:10.1175/JCLI-D-11-00015.1.

Rojas, O., Vrieling, A., and Rembold, F. (2011). Assessing drought probability for agricultural areas in Africa with coarse resolution remote sensing imagery. Remote Sensing of Environment, 115, 343–352.

Roy, D.P. (1997). Investigation of the maximum Normalized Difference Vegetation Index (NDVI) and the maximum surface temperature (Ts) AVHRR compositing procedures for the extraction of NDVI and Ts over forest. International Journal of Remote Sensing, 18(11):2383–2401.

Rubio, E., Caselles, V., and Badenas, C. (1997). Emissivity measurements of several soils and vegetation types in the 8-14 micrometer wave band: Analysis of two field methods. Remote Sensing of Environment, 59:490–521.

Rubio, E., Caselles, V., Coll, C., Valour, E., and Sospedra, F. (2003). Thermal-infrared emissivities of natural surfaces: Improvements on the experimental set-up and new measurements. International Journal of Remote Sensing, 24(24):5379–5390.

Sabol, D.E., Gillespie, A.R., Abbott, E., & Yamada, G. (2009). Field validation of the ASTER Temperature-Emissivity Separation algorithm. Remote Sensing of Environment, 113:2328-2344.

Sakai, S., Ito, A., Umetani, K., Iizawa, I., and Onishi, M. (2009). A practical pyrgeometer using the representative angle. Journal of Atmospheric and Oceanic Technology, 26(3):647–655.

Salisbury, J.W., and D'Aria, D. M. (1992). Emissitivity of terrestrial materials in the 8-14 micrometer atmospheric window. Remote Sensing of Environment, 42:83–106.

Salisbury, J,W. (1998). Spectral measurements field guide. Technical Report ADA362372, Earth Satellite Corporation.

Sandholt, I., Rasmussen, K., and Andersen, J. (2002). A simple interpretation of the surface temperature / vegetation index space for assessment of surface moisture status. Remote Sensing of Environment, Vol. 79, pp. 213–224.

Schädlich, S., Göttsche, F.-M., and Olesen, F.-S. (2001). Influence of Land Surface Parameters and Atmosphere on METEOSAT Brightness Temperatures and Generation of Land Surface Temperature Maps by Temporally and Spatially Interpolating Atmospheric Correction. Remote Sensing of Environment, 75:39–46.

Schneider, P., Ghent, D., Corlett, G., Prata, F., and remedies, J. (2012). AATSR validation: LST validation protocol. Internal publication, UL-NILU-ESA-LST-LVP Issue 1 Revision 0, page 1-39. http://lst.nilu.no/Portals/73/Docs/Reports/UL-NILU-ESA-LST-LVP-Issue1-Rev0-1604212.pdf.

Schneider, P., and Hook, S.J. (2010). Space observations of inland water bodies show rapid surface warming since 1985. Geophysical Research Letters, 37.

Schott, J. R., Hook, S. J., Barsi, J. A., Markham, B. L., Miller, J., Padula, F.P., and Raqueno, N.G. (2012). Thermal infrared radiometric calibration of the entire Landsat 4, 5, and 7 archive (1982–2010). Remote Sensing of Environment, 122:41–49.

Schmugge, T., and Ogawa, K. (2006). Validation of emissivity estimates from ASTER and MODIS data. Proceedings of 2006 International Geoscience and Remote Sensing Symposium (pp. 260–262).

Semmens, K.A., Anderson, M.C., Kustas, W.P., Gao, F., Alfieri, J.G., McKee, L., Prueger, J.H., Hain, C.R., Cammalleri, C., Yang, Y., Xia, T., Sanchez, L., Alsina, M.M., and Velez, M. (2016). Monitoring daily evapotranspiration over two California vineyards using Landsat 8 in a multi-sensor data fusion approach. Remote Sensing of Environment, 185:155-170.

Singh, R.P., Roy, S., and Kogan, F. (2003). Vegetation and temperature condition indices from NOAA AVHRR data for drought monitoring over India. International Journal of Remote Sensing, 20(22):4393–4402.

Snyder, W. C., Wan, Z., Zhang, Y., and Feng, Y. -Z. (1998). Classification-based emissivity for land surface temperature measurement from space. International Journal of Remote Sensing, 19(14), 2753–2774.

Sobrino, J. S. and Caselles, V., (1993). A field method for measuring the thermal infrared emissivity. ISPRS Journal of Photogrammetry and Remote Sensing, 48:24–31.

Sobrino, J.A. and Cuenca, J. (1999). Angular Variation of Thermal Infrared Emissivity for Some Natural Surfaces from Experimental Measurements. Applied Optics, 1999. 38:18, 3931–3936.

Sobrino, J.A. and El Kharraz, MH. (1999). Combining afternoon and morning NOAA satellites for thermal inertia estimation: 1. Algorithms and its testing with Hydrologic Atmospheric Pilot Experiment-Sahel data. Journal of Geophysical Research, 104. D8, 9445– 9453.

Sobrino, J.A., Jiménez-Munoz, J. C., and Verhoef, W. (2005). Canopy directional emissivity: Comparison between models. Remote Sensing of Environment, 99, 304–314.

Sobrino, J.A., Jiménez-Muñoz, J. C., Balick, L., Gillespie, A.R., Sabol, D. A., and Gustafson, W. T. (2007). Accuracy of ASTER level-2 thermal-infrared standard products of an agricultural area in Spain. Remote Sensing of Environment, 106, 146–153.

Sobrino, J. A., Oltra-Carrió, R., Soria G., Jiménez-Muñoz, J. C., Franch, N., Hidalgo, V. *et al.* (2013). Evaluation of the surface urban heat island effect in the city of Madrid by thermal remote sensing. International Journal of Remote Sensing, 34, 3177-3192.

Sobrino, J. A., and Skokovic, D. (2016). Permanent Stations for Calibration/Validation of Thermal Sensors over Spain, Data, 1, 10; doi:10.3390/data1020010.

Sobrino, J. A., Del Frate, F., Drusch, M., Jiménez-Muñoz, J. C., Manunta, P., Regan, A. (2016). Review of Thermal infrared applications and requirements for future high-resolution sensors, IEEE Transactions on Geoscience and Remote Sensing, 54, 2963-2972.

Stöckli, R. (2013). The HelioMont Surface Solar Radiation Processing, Scientific Report MeteoSwiss, 93, ISSN: 1422–138, 122 pp.

Suarez, M., and Bacmeister, J., 2015: Development of the GEOS-5 atmospheric general circulation model: evolution from MERRA to MERRA2, Geoscientific Model Development, 8, 1339-1356.

Theocharous, E., Usadi, E., and Fox, N.P. (2010). CEOS comparison of IR brightness temperature measurements in support of satellite validation. Part I: Laboratory and ocean surface temperature comparison of radiation thermometers. NPL REPORT OP 3. Technical Report ISSN: 1754-2944, National Physical Laboratory, Teddington, UK.

Theocharous, E., Fox, N. Göttsche, F., Hoyer, J. L., Wimmer, W., and Nightingale, T. (2016). Fiducial Reference Measurements for Validation of Surface Temperature from Satellites (FRM4STS) Technical Report TR-1: Procedures and Protocols for the verification of TIR FRM Field Radiometers and Reference Blackbody Calibrators. Reference: OFE- D80-V1-Iss-3-Ver-1-FINAL, 104 pages.

Tonooka, H. (2005). Accurate atmospheric correction of ASTER thermal infrared imagery using the WVS method, IEEE Transactions on Geoscience and Remote Sensing, vol. 43, pp. 2778-2792.

Trigo, I.F., Boussetta, S., Viterbo, P., Balsamo, G., Beljaars, A., Sandu, I. (2015). Comparison of model land skin temperature with remotely sensed estimates and assessment of surface-atmosphere coupling, J. Geophys. Res., 120, doi: 10.1002/2015JD023812.

Trigo, I. F., Monteiro, I. T., Olesen, F., and Kabsch, E. (2008). An assessment of remotely sensed land surface temperature. Journal of Geophysical Research, [Atmospheres], 113, http://dx.doi.org/10.1029/2008JD010035 D17108.

Unsworth, M.H. (1975). Long-wave radiation at the ground. II. Geometry of interception by slopes, solids and obstructed planes. Quarterly Journal of the Royal Meteorological Society, 101, 25–34.

Uppala, S.M., Kållberg, P.W., Simmons, A.J., Andrae, U., Da Costa Bechtold, V., Fiorino, M., Gibson, J.K., Haseler, *et al.* (2005). The ERA-40 re-analysis. Quarterly Journal of the Royal Meteorological Society 131, 2961-3012.

Wan, Z., and Dozier, J. (1996). A generalized split-window algorithm for retrieving land surface temperature from space. IEEE Transactions on Geoscience and Remote Sensing, 34, 892–905.

Wan, Z., Zhang, Y., Zhang, Q., and Li, Z.-L. (2002). Validation of the land-surface temperature products retrieved from Terra Moderate Resolution Imaging Spectroradiometer data. Remote Sensing of Environment, 83:163–180.

Wan, Z. (2008). New refinements and validation of the MODIS land-surface temperature / emissivity products. Remote Sensing of Environment, 112, 59–74.

Wan, Z., and Li, Z. -L. (2008). Radiance-based validation of the V5 MODIS land-surface temperature product. International Journal of Remote Sensing, 29, 5373–5393.

Wan, Z. (2014). New refinements and validation of the collection-6 MODIS land-surface temperature/emissivity product. Remote Sensing of Environment, 140, 36–45, http://dx.doi.org/10.1016/j.rse.2013.08.027.

Wang, W., Liang, S., and Meyers, T. P. (2008). Validating MODIS land surface temperature products using long-term nighttime ground measurements. Remote Sensing of Environment, 112, 623–635.

Wang, K., and Liang, S. (2009). Evaluation of ASTER and MODIS land surface temperature and emissivity products using long-term surface longwave radiation observations at SURFRAD sites. Remote Sensing of Environment, 113(7), 1556–1565.

Wang, Z., Schaaf, C. B., Strahler, A. H., Chopping, M. J., Román, M.O., Shuai, Y., *et al.* (2014). Evaluation of MODIS albedo product (MCD43A) over grassland, agriculture and forest surface types during dormant and snow-covered periods. Remote Sensing of Environment, 140, 60–77.

Wolfe, R.E., Lin, G., Nishihama, M., Tewari, K.P., Tilton, J.C., and Isaacman, A.R. (2013). Suomi NPP VIIRS prelaunch and on-orbit geometric calibration and characterization. Journal of Geophysical Research: Atmospheres, 2013JD020508, 10.1002/jgrd.50873.

Xu, H., Yu, Y., Tarpley, D., Göttsche, F.-M and Olesen, F.-S. (2014), Evaluation of GOES-R Land Surface Temperature Algorithm Using SEVIRI Satellite Retrievals with In Situ Measurements. IEEE Transactions on Geoscience and Remote Sensing, Vol. 52, No. 7, doi: 10.1109/TGRS.2013.2276426.

Yu, Y., Privette, J. L., and Pinheiro, A. (2005). Analysis of the NPOESS VIIRS Land Surface Temperature algorithm using MODIS data. IEEE Transactions on Geoscience and Remote Sensing, Vol. 43, No. 10, 2340-2350.

Zheng, W., Wei, H., Wang, Z., Zeng, X., Meng, J., Ek, M., Mitchell, K. and Derber, J. (2012). Improvement of daytime land surface skin temperature over arid regions in the NCEP GFS model and its impact on satellite data assimilation. J. Geophys. Res, 117, D06117, doi: 10.1029/2011JD015901.

Zhou, L., Dickinson, R.E., Tian, Y., Jin, M., Ogawa, K., Yu, H., and Schmugge, T. (2003). A sensitivity study of climate and energy balance simulations with use of satellite-derived emissivity data over Northern Africa and the Arabian Peninsula. Journal of Geophysical Research-Atmospheres, 108, 4795.

Zorer, R., Rocchini, D., Metz, M., Delucchi, L., Zottele, F., Meggio, F., and Neteler, M. (2013). Daily MODIS Land Surface Temperature Data for the Analysis of the Heat Requirements of Grapevine Varieties. IEEE Transactions on Geoscience and Remote Sensing, 51, 2128-2135.